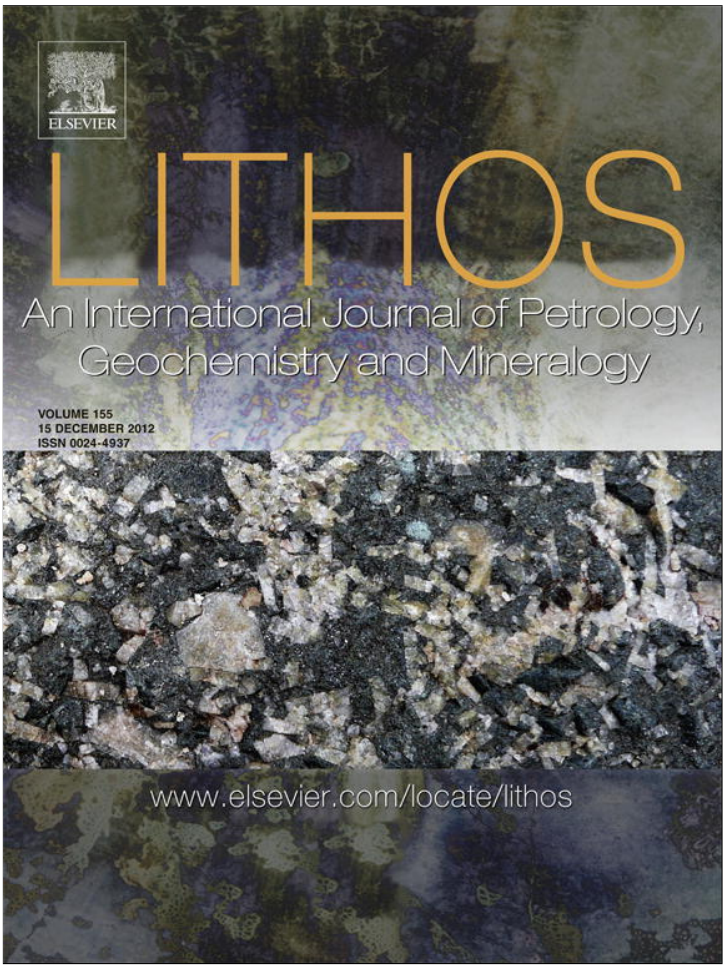

Lithos 155 (2012) 201–217

Contents lists available at SciVerse ScienceDirect

Lithos

journal homepage: www.elsevier.com/locate/lithos

Late Permian appinite–granite complex from northwestern Liaoning, North China Craton: Petrogenesis and tectonic implications

Xiaohui Zhang [a,*], Fuhong Xue [a,b], Lingling Yuan [a,b], Yuguang Ma [a], Simon A. Wilde [c]

[a] State Key Laboratory of Lithospheric Evolution, Institute of Geology and Geophysics, Chinese Academy of Sciences, Beijing 100029, China
[b] University of Chinese Academy of Sciences, Beijing 100039, China
[c] Department of Applied Geology, Curtin University, Perth, Western Australia, Australia

ARTICLE INFO

Article history:
Received 3 May 2012
Accepted 10 September 2012
Available online 17 September 2012

Keywords:
Late Permian
Appinite–granite suite
Geochemistry
Petrogenesis
North China Craton

ABSTRACT

The appinite–granite suite commonly occurs within post-subduction regimes during the final stage of an orogeny and thus holds the key to monitoring critical geodynamic and crustal evolutionary processes. The present zircon U–Pb dating and geochemical study documents the Late Permian appinite–granite complex from northwestern Liaoning, North China Craton. The hornblende-rich appinitic rocks have an SiO_2 range from 41.8 to 53.4%, moderate to high alkali contents, enrichment in large ion lithophile elements and depletion in high field strength elements, with initial $^{87}Sr/^{86}Sr$ ratios of 0.7066 to 0.7128, $\varepsilon_{Nd}(t)$ of −8.3 to −13.3 and zircon $\varepsilon_{Hf}(t)$ from −10.1 to −18.7. These features suggest that their generation most likely involves metasomatism of mantle peridotites by sediment-derived liquids related to subduction and a later partial melting. The associated monzogranites range in SiO_2 from 72.6 to 75.0% and exhibit a high-K calc-alkaline character, with high Sr–Ba abundances and elevated Sr/Y and La/Yb ratios. Such potassic adakitic signatures, plus their evolved isotopic compositions ($^{87}Sr/^{86}Sr_i$ = 0.7063 to 0.7066, $\varepsilon_{Nd}(t)$ = −15.6 to −16.3, zircon $\varepsilon_{Hf}(t)$ = −16.5 to −18.8), are consistent with partial melting of mixed protoliths including newly underplated enriched mafic lower crust and minor old lower crustal materials. Such a mafic and felsic magma association not only attests to a heterogeneously enriched sub-continental lithospheric mantle beneath the northern North China Craton, but also indicates reworking within a post-orogenic transcurrent regime of lithospheric delamination. The temporal coincidence of the present appinite–granite complex with regional transcurrent fault activity leads to the further suggestion that such mafic–felsic magmatic suites could provide spatial markers for monitoring important post-orogenic structural and geodynamic processes.

1. Introduction

Correctly identifying the magmatic record of mantle and crustal processes is essential for understanding the mechanisms by which the continental crust evolves along convergent plate margins. In this regard, the enigmatic appinite–granite association stands out among the various combinations of mafic and felsic magmas because of its distinctive geochemical characteristics and capabilities for monitoring some critical geodynamic events. At the mafic end of this magmatic spectrum, the appinitic suite was firstly described from the Appin district of Scotland (Bailey and Maufe, 1916) and has subsequently been documented from numerous calc-alkaline batholiths worldwide (Atherton and Ghani, 2002; Ayrton, 1991; Bowes and Košler, 1993; Castro et al., 2003; Fowler and Henney, 1996; Fowler et al., 2001, 2008; Pitcher, 1997; Rogers and Dunning, 1991; X.H. Zhang et al., 2012a; Ye et al., 2008). It has been taken to represent a wide variety of mafic rocks typified by hydrous mineral assemblages of hornblende and biotite and by an overall andesitic to basaltic composition of calc-alkaline to shoshonitic affinity. The rocks are typically coarse-grained and the suite generally forms the mafic precursor of granitoid batholiths and thus testifies to mantle involvement in granite genesis (Atherton and Ghani, 2002; Bea et al., 1999; Castro et al., 2003; Fowler and Henney, 1996; Fowler et al., 2001, 2008; Pitcher, 1997; Ye et al., 2008). On the other hand, the felsic end-members in the appinite–granite suite commonly have a high Ba–Sr (Fowler and Henney, 1996; Fowler et al., 2001, 2008; Ye et al., 2008) or high Sr/Y adakitic geochemical affinity (Moyen, 2009), possibly reflecting a range of processes but mostly implying high-pressure melting (Moyen, 2009). Moreover, particularly remarkable for the appinite–granite association is its close spatial/temporal and genetic connection with transcurrent fault movements (Hutton and Reavy, 1992; Rogers and Dunning, 1991) and critical geodynamic processes like post-subduction slab break-off or delamination (Atherton and Ghani, 2002; Neilson et al., 2009; Ye et al., 2008) during the final stage of an orogeny. Therefore, a contemporaneous appinite–granite

* Corresponding author at: State Key Laboratory of Lithospheric Evolution, Institute of Geology and Geophysics, Chinese Academy of Sciences, P.O. Box 9825, Beijing 100029, China. Tel.: +86 10 82998540.
E-mail address: zhangxh@mail.iggcas.ac.cn (X. Zhang).

0024-4937/$ – see front matter © 2012 Elsevier B.V. All rights reserved.
http://dx.doi.org/10.1016/j.lithos.2012.09.002

suite in ancient continental tracts can not only allow fingerprinting of important geodynamic processes, but also help in understanding crustal differentiation mechanisms along convergent plate margins.

The northern part of the North China Craton (NCC) was a convergent plate margin during the Paleozoic and experienced a metacratonization process associated with the closure of the Paleo-Asian Ocean in the Central Asian orogenic belt (CAOB), mainly in the form of multiple episodes of Paleozoic magmatism (Zhang and Zhai, 2010) and structural deformations (Cui et al., 2002; Hu et al., 2003; Wan, 2012; Zhang et al., 2005). A number of recent studies have been conducted to establish the sequence of these magmatic events and to resolve their tectonic affiliation with evolving orogenic processes in the neighboring orogenic belt (Chen et al., 2009; S.H. Zhang et al., 2009a, 2009b; Zhang et al., 2010a, 2011a; X.H. Zhang et al., 2012a). However, controversies still persist concerning the exact regime and crustal evolutionary scenario during the Late Permian, with some advocating an active continental arc setting (S.H. Zhang et al., 2009a, 2009b) whereas others consider it as a post-collisional extensional regime (Zhang and Zhai, 2010; Zhang et al., 2008a, 2008b). This is partly due to the concentration of the most current magmatic studies in the western segment of the belt, and partly to the lack of any initiative in decoding essential tectonic barcodes from related magmatism in most current research strategies.

Therefore, further spatial/temporal and tectonic refinements in studying the Paleozoic magmatism at the northern margin of the NCC are essential for the ongoing reconstruction of Asia. In this paper, we present new zircon U–Pb age, whole-rock geochemistry and Sr–Nd isotopes, and in situ zircon Hf isotopic compositions for the Late Permian mafic and felsic intrusions from northwestern Liaoning along the eastern segment of the northern NCC, with the aims of constraining their petrogenesis, probing their tectonic environment and providing a case study of continental crustal evolution through the characterization of coeval mafic and felsic magmas.

2. Geological setting

The NCC is flanked by the CAOB to the north and the Qinling–Dabie–Sulu orogenic belt to the south (Fig. 1a). It can be divided into the Western and Eastern Blocks with the intervening Trans-North China orogen (TNCO) on the basis of geochronological,

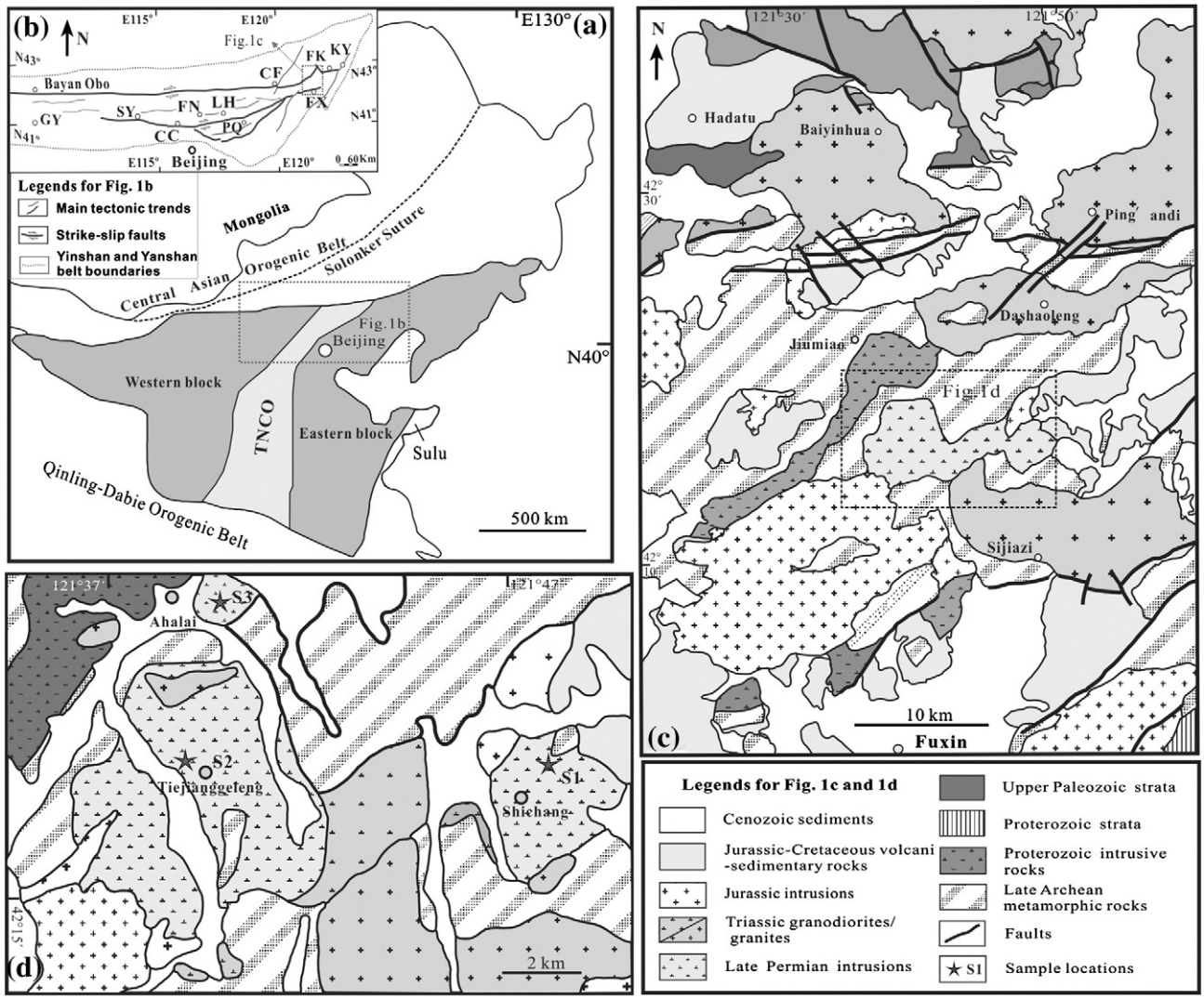

Fig. 1. (a) Simplified map showing major tectonic units of the North China Craton. (b) Map showing the main faults in the northern North China Craton. Abbreviated city names are: GY = Guyang; SY = Shangyi; FN = Fengning; LH = Longhua; CC = Chicheng; PQ = Pingquan; CF = Chifeng; FX = Fuxin; FK = Faku; KY = Kaiyuan. (c) Geological sketch map of northwestern Liaoning. (d) Geological sketch map of the Tiejianggeleng and Shichang plutons, with the sample locations shown. The samples collected at each locality are the following: S1: FX06-15, FX06-16, FX06-17, FX06-18, FX06-19, FX06-20, FX06-21, FX06-22, FX06-23, FX06-24; S2: FX06-52, FX06-54; S3: FX06-57, FX06-58, FX06-59, FX06-61, FX06-62, FX06-65, FX06-66, FX06-73, FX06-74, FX06-75.
(a) is from Zhao et al. (2001), (b) is modified after Davis et al. (2001), Cui et al. (2002), and Wan (2012) and (c) is modified from LBGMR (1971).

lithological, geochemical and metamorphic P–T–t path studies of the basement rocks (Zhao et al., 2001, 2005) (Fig. 1a). These two continental blocks are widely considered to have an independent Late Archean to Early Paleoproterozoic history and collide to form a coherent craton at ~1.85 Ga (Zhao et al., 2001). The Western Block mainly consists of Neoarchean to Paleoproterozoic metasedimentary rocks that unconformably overlie the Archean basement. The Eastern Block has a basement of dominantly Archean tonalite–trondhjemite–granodiorite (TTG) gneisses (3.1–3.8 Ga) and 2.5 Ga granitoids, with minor Archean supracrustal rocks. Post-cratonization cover includes the Mesoproterozoic clastic sedimentary succession of the Changcheng System, Cambrian to Middle Ordovician marine sedimentary rocks, Carboniferous–Permian continental clastic rocks and Mesozoic basin deposits (Kusky et al., 2007; Zhao et al., 2001).

Unlike most other Archean cratons, the NCC underwent widespread tectono-thermal reactivation during the Phanerozoic, resulting in lithospheric thinning and delamination (Menzies et al., 1993; Wu et al., 2005; Yang et al., 2008a). To the north of the NCC, the roughly east–west trending CAOB represents a large accretionary orogen with various components, including island arcs, oceanic islands, accretionary wedges, oceanic plateaux and micro-continents (Windley et al., 2007; Xiao et al., 2003). The northern China–Mongolia tract covers a vast area from southern Mongolia to northern China along the central-eastern segment of the orogenic belt, with the Solonker suture zone marking final closure of the Paleo-Asian Ocean (Fig. 1a) (Jian et al., 2010; Xiao et al., 2003). The NCC and the southern Mongolia terranes were amalgamated prior to this closure and behaved as the combined North China–Mongolian plate (Davis et al., 2001; Zhang et al., 2010b).

The northern NCC extends from southern Inner Mongolia through Beijing Municipality and Hebei Province to northern and western Liaoning Province, and is tectonically equivalent to the Yinshan–Yanshan orogenic belt (Davis et al., 2001) (Fig. 1b). The Bayan Obo–Chifeng–Kaiyuan fault marks its northern boundary (Davis et al., 2001; Xiao et al., 2003; X.H. Zhang et al., 2012b) (Fig. 1b). Associated faults include the Chuanjing–Bulutai Fault at Guyang in southern Inner Mongolia (Zhang et al., 2011a), the Shangyi–Chicheng Fault (Hu et al., 2003), the Pingquan–Gubeikou Fault (Davis et al., 2001) and the Fengning–Longhua Fault (Wan, 2012) in Hebei Province, together with several ductile shear zones in western and northern Liaoning (Zhang et al., 2002, 2005). These faults were possibly initiated in the Paleoproterozoic (Cui et al., 2002; Davis et al., 2001) and subsequently experienced later reactivation. Several structural and geochronological studies on several of them have established multi-stage Phanerozoic events, including Devonian (Hu et al., 2003), Early Permian (Cui et al., 2002), Late Permian to Early Triassic (Hu et al., 2003; Wan, 2012; Zhang et al., 2005), Late Triassic (Zhang et al., 2002) and Late Jurassic (Davis et al., 2001) activity.

During the Late Paleozoic to Early Mesozoic, the northern NCC underwent several magmatic events (Zhang and Zhai, 2010, and references therein). Recent studies in the western and central parts of this region have identified Middle Devonian mafic–ultramafic complexes with ages from 395 to 390 Ma (S.H. Zhang et al., 2009a) and alkaline intrusions at c. 410 Ma (Zhang et al., 2010a), Carboniferous calc-alkaline plutons (S.H. Zhang et al., 2009b) and appinitic suites with ages from 325 to 300 Ma (X.H. Zhang et al., 2012a), Early Permian mafic–ultramafic complex and high-K calc-alkaline I- and A-type granitoids (Chen et al., 2009; Zhang and Zhai, 2010; S.H. Zhang et al., 2009a; Zhang et al., 2011a), and the latest Permian to Early Triassic high-K calc-alkaline to alkaline intrusive rocks with ages from 254 to 237 Ma (S.H. Zhang et al., 2009b; Zhang et al., 2010b).

Northwestern Liaoning is located along the north-eastern margin of the NCC (Fig. 1b and c). Its basement is characterized by lower amphibolite to granulite facies Archean to Paleoproterozoic gray tonalitic gneisses and greenstones of the Jianping complex and Neoproterozoic low-grade metamorphic to unmetamorphosed rock sequences of the Changcheng group. The Jianping complex records a major magmatic event at 2589–2495 Ma and granulite facies metamorphism at ca. 2490 Ma (Liu et al., 2011; Wang et al., 2011). Typical Phanerozoic cover sequences include sporadically distributed Permo-Carboniferous non-marine sequences and well-exposed Jurassic–Lower Cretaceous fluvial–lacustrine strata resting unconformably on the Archean and Paleoproterozoic basement.

Among numerous E–W, NE–SW and NNE-trending fault systems present in the study area, the most prominent E–W trending ones constitute a part of the Chifeng–Kaiyuan cratonic boundary fault system (Fig. 1b). This fault zone experienced repeated activation, however, its poly-phase structural history has been poorly constrained due to complicated overprinting effects from the transposition of multiple deformations and other geologic events including magmatism, erosion and sedimentation (Zhang et al., 2002).

Multiple phases of Phanerozoic igneous rocks intrude Archean and Paleoproterozoic metamorphic rocks in northwestern Liaoning (Fig. 1c). However, they were not well constrained prior to our ongoing geochronological studies. Based on the intrusive relationships and mineralogical and geochemical patterns, they appear to form during three major episodes: the Hercynian, Indonisian (Triassic) and Yanshanian (Jurassic and Cretaceous) (Chi and Lin, 1999; LBGMR, 1971, 1996; Lin, 1996). The first episode is represented by a few Hercynian dioritic to granitic plutons; the second episode by voluminous Middle–Late Triassic plutonic rocks with ages from 238 to 219 Ma (X.H. Zhang et al., 2012b); and the third episode by a number of Middle to Late Jurassic granitic intrusions. They are variously covered by the Jurassic to Cretaceous volcano-sedimentary strata.

3. Field relations and petrography

The Hercynian appinite–granite complex, as represented by the Tiejianggeleng (TJGL) and Shichang (SC) plutons, is located approximately 50 km to the north of Fuxin City (Fig. 1d). They mainly occur as poorly-exposed stocks and wide dikes intruding Archean and Paleoproterozoic metamorphic rocks (LBGMR, 1971, 1996; Lin, 1996), and associated with younger granitic intrusions. The TJGL pluton has an area of ~40 km^2 while the SC pluton covers an area of ~30 km^2 (Lin, 1996). Both plutons are locally deformed with well-developed foliations at their margins. They are predominantly composed of hornblende-rich mafic components, with minor amounts of felsic units. Owing to poor field exposure and severe weathering, we were able to sample only a few fresh rocks from an iron ore quarry (for the TJGL pluton) and along a few dry river-valleys (for both).

The mafic components are commonly hornblende diorite and monzodiorite, with medium- to coarse-grained intergranular textures. Typical samples comprise euhedral to subhedral amphibole (25–45%) and plagioclase (25–60%), with subhedral clinopyroxene (0–5%) and biotite (0–5%), minor amounts of alkali feldspar and quartz. Accessory phases include euhedral magnetite and ilmenite, subhedral apatite, zircon and titanite. Amphiboles show a wide range of X_{Mg} [= Mg/(Fe + Mg); 0.45–0.77] and mainly belong to the magnesio-hornblende and actinolite groups (Leake et al., 1997). They are locally altered to epidote. Plagioclase has an andesine to labradorite composition ($An_{35-57}Ab_{43-63}Or_{0-2}$), with weak to moderate sericitization. Clinopyroxene commonly occurs as relics in amphibole and is classified as augite and diopside with the composition $Wo_{25-43}En_{38-56}Fs_{13-23}$. K-feldspar occurs as a subhedral to anhedral interstitial phase, with a composition of $Or_{89-99}Ab_{1-7}$.

The felsic rocks mainly comprise fine- to medium-grained, equigranular biotite monzogranite. Typical samples contain 25–30% K-feldspar, 30–40% plagioclase, 20–30% quartz, 5–12% biotite, and accessory zircon, apatite, magnetite and rutile. K-feldspar mainly occurs as perthitic orthoclase ($Qr_{85-97}Ab_{3-15}$) with large subhedral to

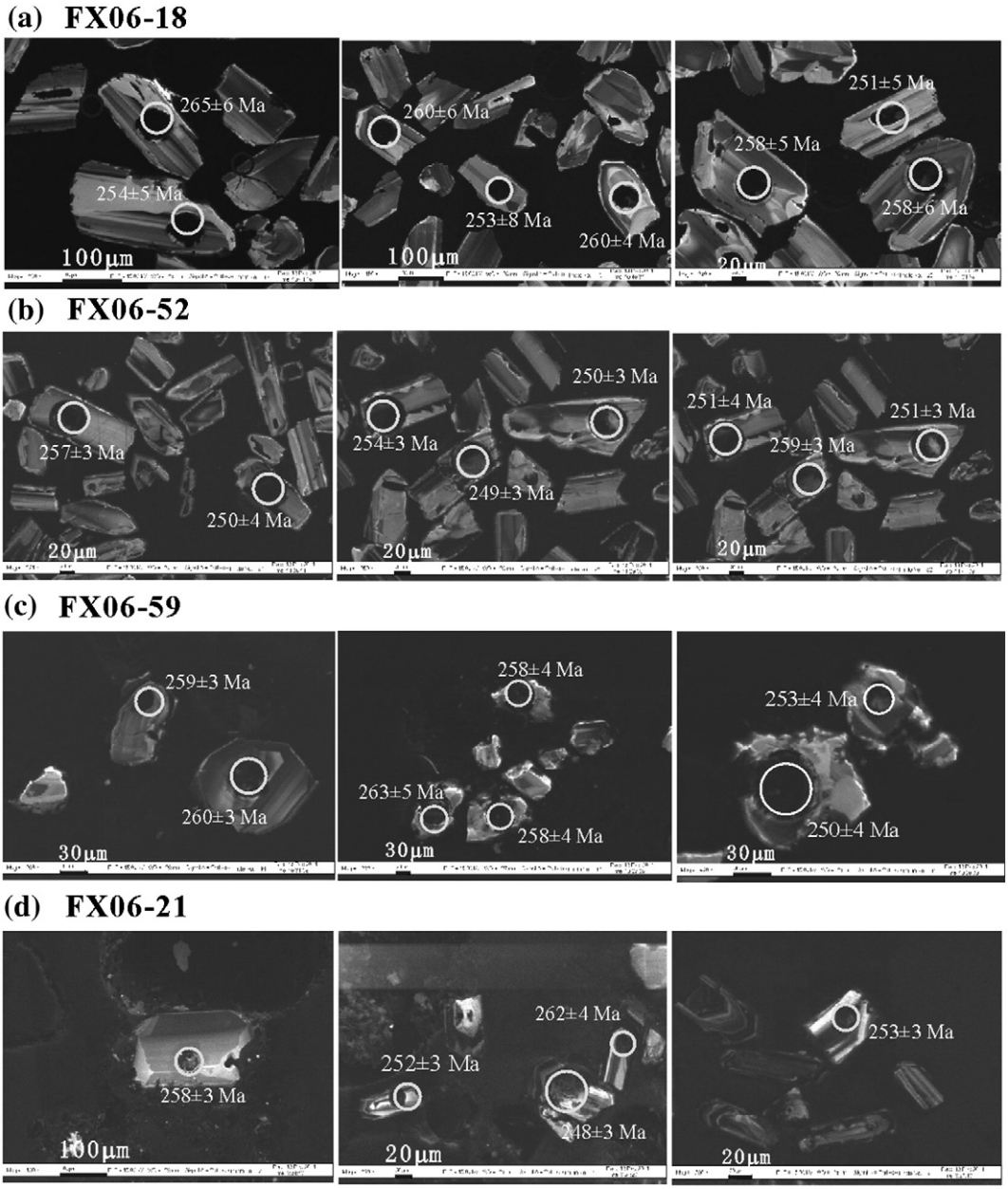

Fig. 2. Cathodoluminescence images of selected dated zircons from the Late Permian appinite–granite pluton from northwestern Liaoning. (a) Sample FX06-18. (b) Sample FX06-52. (c) Sample FX06-59. (d) Sample FX06-21.

euhedral crystals. Plagioclase is chiefly oligoclase in composition ($An_{11-25}Ab_{64-95}Or_{0-2}$). Quartz mainly forms aggregates that make up large phenocrysts. Subhedral to anhedral biotite (X_{Mg} = 0.42–0.46) is interstitial to K-feldspar and quartz.

4. Analytical methods

For major element compositions of minerals, we used a JEOL JXA-8100 electron microprobe at the Institute of Geology and Geophysics, Chinese Academy of Sciences (IGGCAS), with operating conditions of 15 kV accelerating voltage, 10 nA beam current and 3 μm spot diameter. Well-defined natural mineral standards were used for calibration. The analytical errors are generally less than 2%.

Zircon separation procedure followed standard density and magnetic separation techniques and they were than handpicked under a binocular microscope. Cathodoluminescence (CL) imaging of zircon was conducted on a JXA-8100 microprobe at IGGCAS prior to analysis in order to identify internal complexities.

Zircons from samples FX06-21 and FX06-59 were dated by LA-ICP-MS at the State Key Laboratory of Geological Processes and Mineral Resources, China University of Geosciences in Wuhan, China. Detailed operating conditions for the laser ablation system and the ICP-MS instrument and data reduction are the same as those described in Liu et al. (2010). Laser sampling was performed using a GeoLas 2005. An Agilent 7500a ICP-MS instrument was used to acquire ion-signal intensities. Helium was used as the carrier gas. Harvard zircon 91500 was used as the standard and silicate glass NIST was used as the reference material. Preferred U–Th–Pb isotopic ratios for 91500 are from Wiedenbeck et al. (1995). The common-Pb corrections were made using the method of Anderson (2002) and the data were processed using the GLITTER (Griffin et al., 2008) and ISOPLOT (Ludwig, 2001) programs.

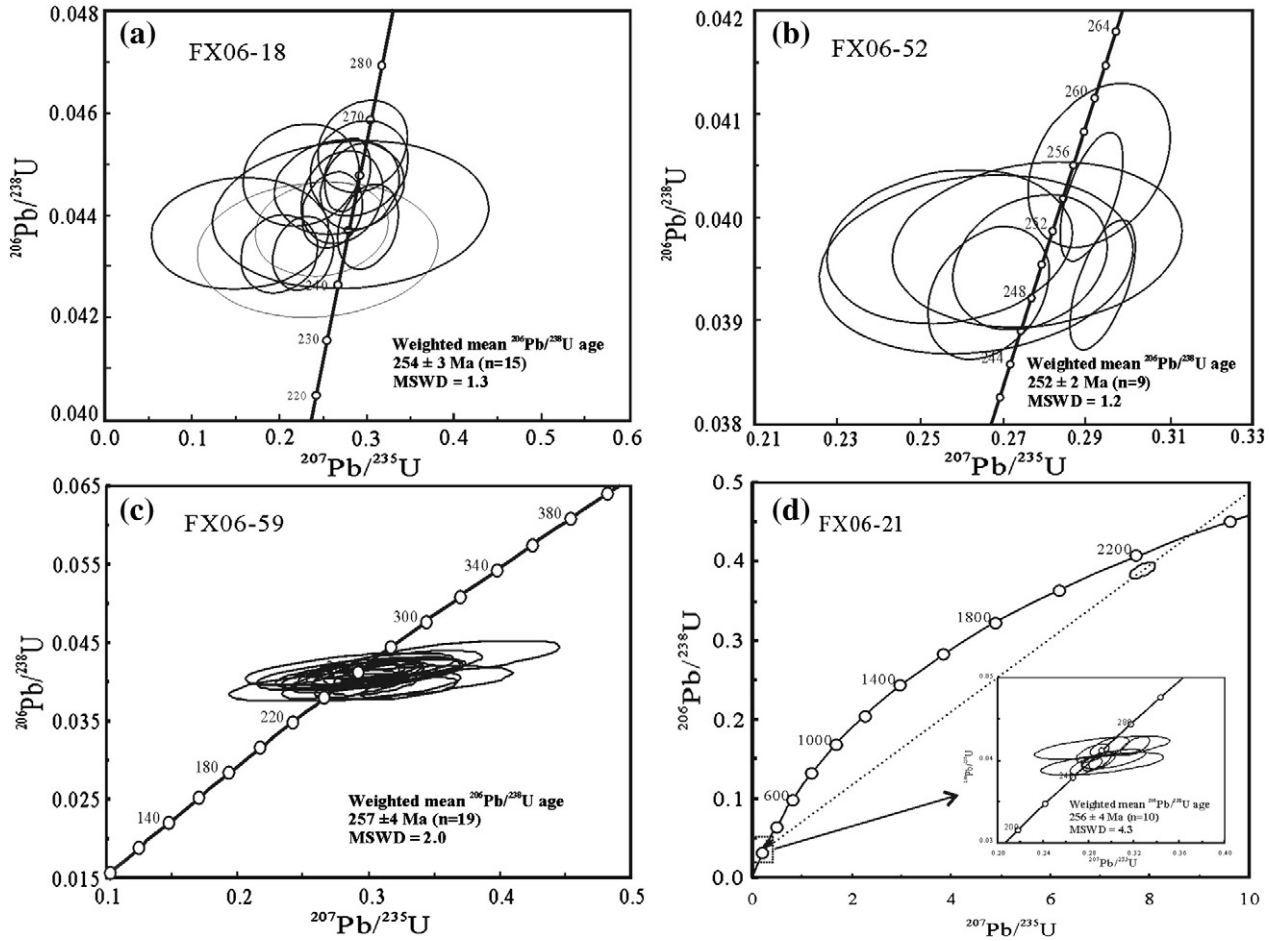

Fig. 3. U–Pb zircon concordia diagrams for the Late Permian appinite–granite complex from northwestern Liaoning. (a) Sample FX06-18. (b) Sample FX06-52. (c) Sample FX06-59. (d) Sample FX06-21.

Zircons from samples FX06-18 and FX06-52 were dated on a SHRIMP II (sensitive high-resolution ion-microprobe) at Curtin University of Technology under standard operating conditions (6-scan cycle, 2 nA primary O_2^- beam, mass resolution ca. 5000). The analytical procedures were the same as those described by Williams (1998), with data processed using the SQUID (1.02) and ISOPLOT programs and corrected for common lead by using the measured ^{204}Pb. Corrections of Pb/U ratios were made by normalization to zircon standard CZ3 ($^{206}Pb/^{238}Pb = 0.0914$, corresponding to an age of 564 Ma). Individual analyses by both LA-ICP-MS and SHRIMP are reported with 1σ uncertainties; whereas weighted mean ages are reported at the 2σ confidence level.

After petrographic examination, selected fresh rock samples were ground in an agate mill to ~200 μm mesh powder for geochemical analyses. Major elements were determined by X-ray fluorescence spectroscopy with a Shimadzu XRF 1500 sequential spectrometer at the IGGCAS, following the analytical procedure described in X.H. Zhang et al. (2012a). The samples were heated in two steps within separate ovens at 105 °C and 1000 °C, respectively, to measure loss on ignition (LOI). The analytical uncertainties are better than 5% as revealed by long-term measurements of Chinese national standards GSR-1 (granite) and GSR-3 (basalt).

For trace element analyses, whole rock powders (40 mg) were dissolved in distilled $HF + HNO_3$ in 15 ml high-pressure Teflon bombs at 200 °C for 5 days, dried and then digested with HNO_3 at 150 °C for 1 day. Dissolved samples were diluted with 1% HNO_3 to 49 ml and 1 ml 500 ppb indium was added to the solution as an internal standard. Trace element abundances were determined by a VG-PQII inductively coupled plasma mass spectrometer (ICP-MS) at the IGGCAS. A blank solution was prepared and the total procedural blank was <50 ng for all trace elements. Precision for all trace elements is estimated to be 5% and accuracy is better than 5% for most elements, monitored by analyses of Chinese national standard samples GSR-1 and GSR-3.

The Rb–Sr and Sm–Nd isotopic analysis followed procedures similar to those described by Yang et al. (2010). Whole rock powders were dissolved in Savillex Teflon screw-top capsules after being spiked with the mixed ^{87}Rb–^{84}Sr and ^{149}Sm–^{150}Nd tracers prior to $HF + HNO_3 + HClO_4$ dissolution. Rb, Sr, Sm and Nd were separated using the classical two-step ion exchange chromatographic method and measured using a Finnigan MAT262 multi-collector thermal ionization mass spectrometer at the IGGCAS. The procedural blank was lower than 300 pg for Rb–Sr and 100 pg for Sm–Nd. The isotopic ratios were corrected for mass fractionation by normalizing to $^{88}Sr/^{86}Sr = 8.375209$ and $^{146}Nd/^{144}Nd = 0.7219$, respectively. The international standard samples, NBS-987 and JNdi-1, were employed to evaluate instrument stability during the period of data collection. The measured values for the BCR-2 Nd standard and BCR-2 Sr standard were $^{143}Nd/^{144}Nd = 0.512613 \pm 0.000012$ (2σ, n = 4) and $^{87}Sr/^{86}Sr = 0.705033 \pm 0.000011$ (2σ, n = 4) during the period of data acquisition.

In situ zircon Hf isotopic analyses were conducted using a Neptune MC-ICP-MS equipped with a 193-nm laser at the IGGCAS, with a spot size of 32 μm and a laser repetition rate of 10 Hz at 100 mJ. The detailed analytical procedure and correction for interferences are similar to those described by Wu et al. (2006a, 2006b). The $^{176}Hf/^{177}Hf$ and $^{176}Lu/^{177}Hf$ ratios of the standard zircon (91500) during analysis were 0.282270 ± 0.000023 (2rn, n = 15) and 0.00028, similar to the commonly accepted $^{176}Hf/^{177}Hf$ ratio of $0.282284 \pm$

Table 1
Major and trace element data for the Late Permian appinite–granite pluton from northwestern Liaoning, North China Craton.

Sample	FX06-15	FX06-16	FX06-17	FX06-18	FX06-19	FX06-20	FX06-52	FX06-54
Longitude	E 121° 47′ 32″						E 121° 38′ 38″	
Latitude	N 42° 15′ 42″						N 42° 17′ 36″	
SiO_2	49.47	51.47	51.94	48.51	49.71	59.58	53.34	46.05
TiO_2	1.70	1.06	1.65	1.22	1.18	0.70	1.41	1.94
Al_2O_3	12.23	20.06	13.04	20.05	19.50	15.36	12.99	12.58
TFe_2O_3	17.79	10.03	15.79	10.64	10.85	5.26	9.20	17.08
MnO	0.24	0.13	0.22	0.09	0.10	0.07	0.16	0.20
MgO	5.88	2.65	5.00	2.69	2.52	5.92	7.21	7.99
CaO	8.71	6.27	8.13	7.82	7.97	5.29	8.37	10.68
Na_2O	2.50	4.48	2.82	4.04	3.98	3.24	3.08	2.04
K_2O	0.77	1.82	0.63	1.74	1.12	2.33	2.21	0.51
P_2O5	0.21	0.79	0.21	0.94	0.94	0.22	0.46	0.11
LOI	0.70	1.32	0.54	1.97	1.50	1.65	1.18	0.70
TOTAL	100.19	100.08	99.98	99.71	99.38	99.62	99.61	99.88
Mg#	39.6	34.4	38.5	33.4	31.5	69.0	60.8	48.1
A/CNK	0.59	0.97	0.65	0.88	0.88	0.88	0.57	0.54
Sc	41.1	6.62	39.4	6.96	6.08	14.3	29.4	47.9
V	375	80.9	349	135	132	119	204	648
Cr	41.0	2.02	38.0	0.42	0.94	317	378	83.0
Co	50.4	14.6	45.3	20.4	19.8	26.9	35.8	58.4
Ni	49.8	3.68	40.3	4.88	4.35	156	104	66.3
Ga	18.1	23.0	19.8	22.8	22.3	18.9	19.4	20.2
Rb	6.45	28.2	10.8	32.0	18.7	58.9	55.1	8.19
Sr	262	1498	316	1401	1394	920	907	489
Y	36.2	17.5	33.9	15.1	13.9	16.3	18.7	19.6
Zr	134	279	122	177	166	162	167	71.4
Nb	8.38	7.84	8.53	7.20	6.74	5.06	12.5	4.10
Cs	0.57	1.61	0.53	3.19	4.21	4.25	0.49	0.51
Ba	267	1335	233	872	639	735	596	183
Hf	3.79	6.60	3.57	4.386	4.11	4.554	4.57	2.28
Ta	0.57	0.37	0.55	0.331	0.30	0.378	1.02	0.25
Pb	4.79	8.64	5.65	9.70	9.91	15.3	7.17	3.08
Th	2.19	2.06	1.72	1.39	1.36	13.8	2.45	0.71
U	0.68	0.35	0.50	0.49	0.45	2.920	1.66	0.18
La	18.4	44.8	19.0	30.8	27.2	39.0	34.9	10.2
Ce	42.3	93.2	44.4	69.0	61.5	80.2	78.0	21.9
Pr	5.73	13.0	6.05	9.95	9.01	9.96	11.6	3.39
Nd	23.9	49.2	24.9	40.0	34.9	38.8	44.6	16.2
Sm	5.83	9.41	6.01	8.14	7.53	7.39	9.27	4.13
Eu	1.57	2.58	1.47	2.43	2.17	1.84	2.40	1.33
Gd	6.12	7.36	5.99	6.44	5.78	5.73	6.76	3.99
Tb	1.08	0.93	1.00	0.81	0.76	0.71	0.87	0.68
Dy	6.71	4.29	6.43	3.68	3.48	3.54	4.30	3.95
Ho	1.44	0.73	1.38	0.59	0.55	0.67	0.78	0.77
Er	3.87	1.68	3.74	1.29	1.24	1.75	1.90	2.11
Tm	0.58	0.21	0.56	0.16	0.15	0.25	0.26	0.31
Yb	3.84	1.23	3.61	0.93	0.87	1.63	1.63	1.94
Lu	0.59	0.16	0.55	0.12	0.12	0.24	0.24	0.28
La_N/Yb_N	3.44	26.2	3.78	23.9	22.5	17.1	15.3	3.80
Eu/Eu*	0.80	0.91	0.74	0.99	0.97	0.83	0.89	0.99

Sample	FX06-57	FX06-58	FX06-59	FX06-61	FX06-62	FX06-65	FX06-66
Longitude	E 121° 39′ 11″						
Latitude	N 42° 19′ 59″						
SiO_2	41.41	49.52	41.84	42.53	42.58	43.41	43.99
TiO_2	2.75	0.50	3.04	3.15	2.85	2.76	2.58
Al_2O_3	15.72	13.34	16.03	15.50	18.06	17.88	18.98
TFe_2O_3	17.34	11.92	16.97	15.66	14.80	14.40	12.91
MnO	0.10	0.17	0.10	0.10	0.08	0.09	0.07
MgO	6.99	10.89	6.48	7.97	6.59	6.25	6.48
CaO	9.78	8.35	10.11	10.38	9.93	9.91	9.58
Na_2O	2.45	1.88	2.52	2.75	2.84	2.94	2.93
K_2O	0.82	0.36	0.73	0.58	0.58	0.66	0.75
P_2O5	0.89	0.27	0.98	0.25	0.24	0.26	0.07
LOI	1.05	2.13	0.86	0.62	0.75	1.00	0.87
TOTAL	99.31	99.33	99.67	99.48	99.30	99.54	99.21
Mg#	44.4	64.4	43.1	50.2	46.9	46.2	49.9
A/CNK	0.69	0.71	0.69	0.65	0.77	0.65	0.82
Sc	37.5	33.0	36.0	41.2	31.1	30.0	29.4
V	541	231	538	474	448	378	377
Cr	0.90	617	0.35	2.06	0.38	1.10	0.36
Co	62.0	48.9	58.3	59.5	55.5	53.8	48.8
Ni	17.1	113	29.5	14.7	28.6	26.4	25.4

Table 1 (*continued*)

Sample	FX06-57	FX06-58	FX06-59	FX06-61	FX06-62	FX06-65	FX06-66
Longitude	E 121° 39′ 11″						
Latitude	N 42° 19′ 59″						
Ga	23.7	15.3	23.4	22.8	23.1	22.8	22.3
Rb	20.9	5.58	12.2	4.91	4.14	9.48	7.87
Sr	981	584	1082	1065	1253	1325	1326
Y	24.6	10.7	25.1	23.5	18.7	18.0	18.0
Zr	51.1	18.8	58.6	55.9	42.7	41.6	43.2
Nb	5.48	0.66	5.54	6.08	5.31	4.61	5.46
Cs	2.31	1.43	0.80	0.51	2.21	1.44	1.43
Ba	388	168	412	346	330	334	400
Hf	1.89	0.68	1.99	2.19	1.61	1.57	1.64
Ta	0.26	0.03	0.28	0.32	0.26	0.24	0.27
Pb	3.19	2.63	3.27	2.59	2.30	2.85	2.80
Th	0.29	0.03	0.24	0.28	0.21	0.21	0.33
U	0.07	0.04	0.09	0.07	0.05	0.048	0.07
La	17.8	7.26	20.8	12.4	10.4	11.4	10.2
Ce	46.1	16.4	49.0	36.9	28.5	28.2	26.9
Pr	7.10	2.54	7.99	5.92	4.85	4.60	4.52
Nd	33.3	11.0	34.6	29.4	22.8	21.6	21.1
Sm	7.96	2.74	8.59	7.99	5.88	5.94	5.56
Eu	2.27	0.77	2.29	2.18	1.89	1.83	1.90
Gd	7.05	2.40	7.33	6.99	5.40	5.42	5.10
Tb	1.05	0.37	1.06	1.00	0.76	0.76	0.75
Dy	5.24	2.07	5.65	5.46	4.04	4.18	3.89
Ho	1.00	0.39	1.02	1.02	0.76	0.75	0.73
Er	2.34	1.05	2.45	2.50	1.84	1.81	1.76
Tm	0.31	0.16	0.32	0.32	0.24	0.24	0.23
Yb	1.75	0.95	1.87	1.88	1.34	1.34	1.30
Lu	0.24	0.15	0.25	0.26	0.18	0.18	0.18
La_N/Yb_N	7.31	5.49	7.97	4.72	5.57	6.12	5.64
Eu/Eu*	0.91	0.90	0.86	0.87	1.01	0.97	1.07
Sample	FX06-21	FX06-22	FX06-23	FX06-24	FX06-73	FX06-74	FX06-75
Longitude	E 121° 47′ 32″				E 121° 39′ 42″		
Latitude	N 42° 15′ 42″				N 42° 20′ 12″		
SiO_2	74.96	72.55	74.06	72.73	73.95	74.15	73.76
TiO_2	0.13	0.24	0.19	0.14	0.15	0.15	0.19
Al_2O_3	13.31	14.30	13.54	14.35	14.14	14.07	14.07
TFe_2O_3	1.09	1.75	1.32	1.25	1.11	1.22	1.34
MnO	0.00	0.01	0.02	0.00	0.01	0.01	0.02
MgO	0.30	0.50	0.32	0.30	0.27	0.30	0.31
CaO	0.69	1.30	1.15	1.01	0.79	0.83	0.94
Na_2O	2.98	3.91	3.74	3.12	3.41	3.10	3.22
K_2O	5.25	4.12	4.58	6.02	5.44	5.72	5.38
P_2O5	0.04	0.10	0.06	0.04	0.05	0.06	0.07
LOI	0.57	0.55	0.48	0.42	0.50	0.56	0.48
TOTAL	99.32	99.33	99.46	99.38	99.82	100.17	99.78
Mg#	35.0	36.2	32.3	31.9	32.5	32.8	31.4
A/CNK	1.12	1.08	1.03	1.06	1.09	1.10	1.10
Sc	1.02	2.08	1.97	0.51	1.69	1.43	2.27
V	8.39	16.7	13.7	9.60	14.4	15.0	14.6
Cr	3.27	2.26	1.96	4.40	3.91	10.1	4.37
Co	5.71	2.70	2.11	1.81	2.02	2.19	2.52
Ni	3.49	2.70	2.04	3.41	11.7	10.4	4.25
Ga	14.1	17.2	16.2	16.7	15.6	15.0	17.3
Rb	94.6	94.2	98.9	104	95.0	86.6	91.5
Sr	289	386	382	442	434	375	482
Y	5.75	7.28	6.38	8.09	4.98	4.41	11.1
Zr	74.4	165	127	108	127	125	182
Nb	8.62	9.15	6.84	7.59	9.88	7.95	15.6
Cs	1.46	1.92	1.36	1.73	1.76	1.66	1.94
Ba	1014	1377	1189	1520	1553	1627	1545
Hf	2.57	4.55	3.82	3.29	3.86	3.62	5.52
Ta	1.17	0.85	0.68	0.84	1.33	0.85	2.11
Pb	31.1	26.1	24.6	30.0	32.5	30.5	35.9
Th	6.02	8.31	7.27	16.7	18.9	16.3	32.6
U	1.47	0.58	0.53	1.21	0.88	0.69	1.30
La	16.6	37.6	26.7	35.9	32.6	30.2	61.2
Ce	26.3	61.1	47.8	66.9	48.6	48.7	103
Pr	3.05	6.75	4.85	7.37	4.97	4.79	9.83
Nd	10.3	20.1	15.5	23.7	15.4	15.0	30.8
Sm	1.97	2.89	2.61	3.89	2.32	2.20	4.46
Eu	0.59	0.64	0.55	0.90	0.49	0.47	0.86

(*continued on next page*)

Table 1 (*continued*)

Sample	FX06-21	FX06-22	FX06-23	FX06-24	FX06-73	FX06-74	FX06-75
Longitude	E 121° 47′ 32″				E 121° 39′ 42″		
Latitude	N 42° 15′ 42″				N 42° 20′ 12″		
Gd	1.50	2.13	1.81	2.70	1.69	1.53	3.52
Tb	0.22	0.25	0.23	0.34	0.22	0.18	0.46
Dy	1.15	1.15	1.13	1.66	1.02	0.88	2.30
Ho	0.21	0.21	0.21	0.29	0.19	0.16	0.44
Er	0.509	0.619	0.62	0.77	0.50	0.43	1.12
Tm	0.071	0.095	0.11	0.12	0.08	0.06	0.16
Yb	0.451	0.622	0.71	0.75	0.51	0.43	0.99
Lu	0.069	0.095	0.11	0.10	0.08	0.07	0.15
La_N/Yb_N	26.4	43.4	27.0	34.1	46.0	50.7	44.2
Eu/Eu*	1.01	0.75	0.74	0.80	0.73	0.74	0.64

Notes: Mg# = 100 × molar Mg/(Mg + Fe) ($TFeO = 0.9 \times TFe_2O_3$); LOI = loss on ignition; A/NCK = Al/Na + Ca + K; $Eu/Eu^* = Eu_N/[(Sm_N + Gd_N)/2]$; N = chondrite normalized to values of Sun and McDonough (1989).

0.000003 (1r) measured using the solution method (Woodhead et al., 2004).

5. Results

5.1. Zircon U–Pb data

Zircon U–Pb data for the Late Permian appinite–granite complex from northwestern Liaoning are listed in the Online Supplemental Table 1. Zircons from three representative mafic rocks (FX06-18, FX06-52 and FX06-59) are mostly clear, euhedral to subhedral, stubby to elongate prisms, with common internal oscillatory or banded zoning in CL images (Fig. 2a, b, c). Fifteen analyses on 15 grains from FX06-18 yield U concentrations from 20 to 141 ppm, Th concentrations from 3 to 236 ppm and Th/U ratios from 0.15 to 1.73. All analyses define a weighted mean $^{206}Pb/^{238}U$ age of 254 ± 3 Ma with an MSWD of 1.3 (Fig. 3a). Nine analyses on 9 grains from sample FX06-52 yield U concentrations from 85 to 761 ppm, Th concentrations from 13 to 1276 ppm and Th/U ratios from 0.12 to 2.0. All analyses define a weighted mean $^{206}Pb/^{238}U$ age of 252 ± 2 Ma with an

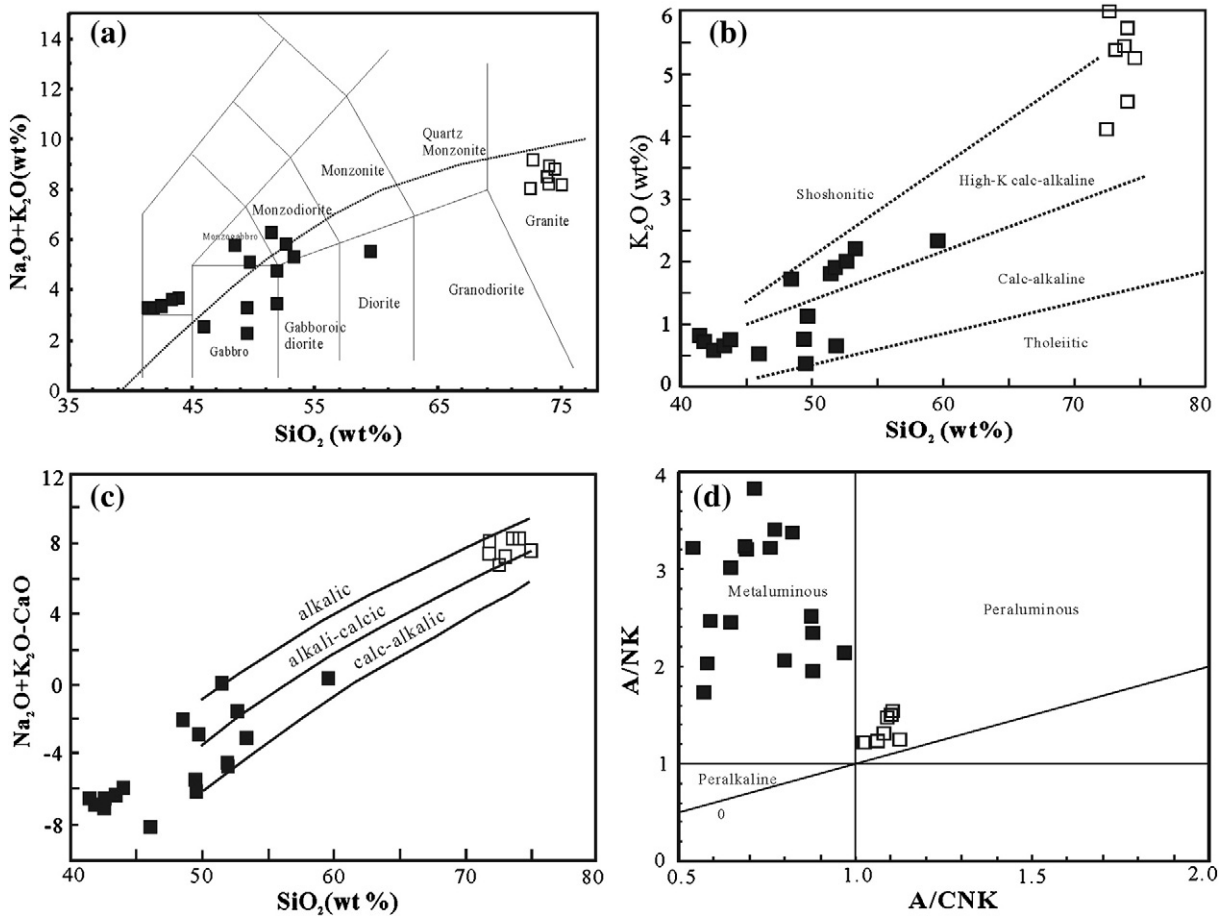

Fig. 4. Classification diagrams for the Late Permian appinite–granite pluton from northwestern Liaoning. (a) Total alkalis vs. silica. (b) Plot of K_2O vs. SiO_2. (c) Plot of ($Na_2O + K_2O - CaO$) vs. SiO_2. (d) Plot of A/NK vs. A/CNK [A/NK = molar ratio of $Al_2O_3/(Na_2O + K_2O)$; A/CNK = molar ratio of $Al_2O_3/(CaO + Na_2O + K_2O)$].
(a) is from Le maitre (2002). The alkaline-tholeiitic division (dotted line) is from Irvine and Barager (1971). (c) is from Frost et al. (2001).

MSWD of 1.2 (Fig. 3b). Nineteen analyses on 19 grains from sample FX06-59 yield U concentrations from 33 to 217 ppm, Th concentrations from 23 to 234 ppm and Th/U ratios from 0.45 to 2.48. All analyses define a weighted mean $^{206}Pb/^{238}U$ age of 257 ± 4 Ma with an MSWD of 2.0 (Fig. 3c).

Zircons from the monzogranite sample FX06-21 are light brown with no inclusions (Fig. 2d). They are 70–180 μm in size and mostly euhedral to subhedral prismatic crystals. In CL images, they show common internal oscillatory zonation (Fig. 2d). Ten measured grains from this sample yield U concentrations from 152 to 1281 ppm, Th concentrations from 152 to 1762 ppm and Th/U ratios from 0.12 to 1.85. Apart from one discordant spot with an inherited $^{207}Pb/^{206}Pb$ age of 2308 Ma, nine analyses form a coherent group with a weighted mean $^{206}Pb/^{238}U$ age of 256 ± 4 Ma (MSWD = 1.5) (Fig. 3d).

5.2. Major and trace elements

Table 1 lists major and trace element abundances in the analyzed samples from the mafic–felsic suite from northwestern Liaoning. The rocks display a clear bimodal geochemical distribution in the total alkali vs. silica plot (Le Maitre, 2002) (Fig. 4a), with most samples plotting in the fields of gabbro-abbroic, diorite-monzogabbro and granite. The mafic samples have low to moderate silica from 41.4 to 53.3%, high contents of total Fe_2O_3 (8.6–17.8%), CaO (6.3–10.4%) and Al_2O_3 (12.22–20.06%), variable abundances of MgO (2.52–10.89%), TiO_2 (0.50–3.15%), K_2O (0.36–2.21%), Cr (1–378 ppm) and V (132–648 ppm). They exhibit a medium to high-K calc-alkaline character on the K_2O vs. SiO_2 plot (Fig. 4b). On the alkali–lime index (MALI = NaO + KO − CaO by wt.) plot of Frost et al. (2001) (Fig. 4c), they range from calc-alkali to alkali-calcic and have an aluminum saturation index [ASI = molar $Al_2O_3/(CaO + K_2O + Na_2O)$] of 0.54 to 0.97 (Fig. 4d) making them metaluminous. They have Mg# from 33 to 66. In Online Supplemental Fig. 1, most samples roughly define a continuous evolution trend: CaO, TiO_2, and $Fe_2O_3^*$ are positively correlated with MgO, whereas Al_2O_3, K_2O, Na_2O, TiO_2, and P_2O_5 are negatively correlated. Likewise, compatible elements such as Sc, Co, Ni and V increase with increasing MgO, whereas Sr, Ba, Pb, Zr, Nb and Y decrease with increasing MgO. Th displays no clear trend with increasing MgO. In addition, Cr is positively correlated with Ni. In terms of other trace elements, the mafic rocks have total REE contents ranging from 48.2 to 229 ppm. In the chondrite-normalized REE diagram (Fig. 5a), they display variable light REE-enriched patterns from moderate ($(La_N/Yb_N = 3.44$ to $7.97)$) in most samples to high ($La_N/Yb_N = 15.3$ to 26.2) in the other five samples, with small negative or positive Eu anomalies ($Eu/Eu^* = 0.75$–1.07; Table 1). In the primitive mantle-normalized spidergram (Fig. 5b), they exhibit positive Rb, Ba, Sr, and Pb anomalies, and negative Nb, Ta, Zr and Hf anomalies.

One diorite sample (FX06-20) is characterized by high contents of Al_2O_3 and MgO, moderate total Fe_2O_3, and low contents of TiO_2 and P_2O_5. It shows high LREE enrichment ($La_N/Yb_N = 17.2$), a small negative Eu anomaly ($Eu/Eu^* = 0.83$) (Fig. 5a), moderately enriched large ion lithophile elements (LILE) and depleted high field strength elements (HFSE) in the primitive mantle-normalized diagrams (Fig. 5b).

The monzogranites have a restricted SiO_2 range from 72.6 to 75.0%, with high Al_2O_3 (13.3–14.3%) and alkalis ($K_2O + Na_2O =$ 8.0–9.14%), and low MgO and TiO_2 concentrations. They exhibit a

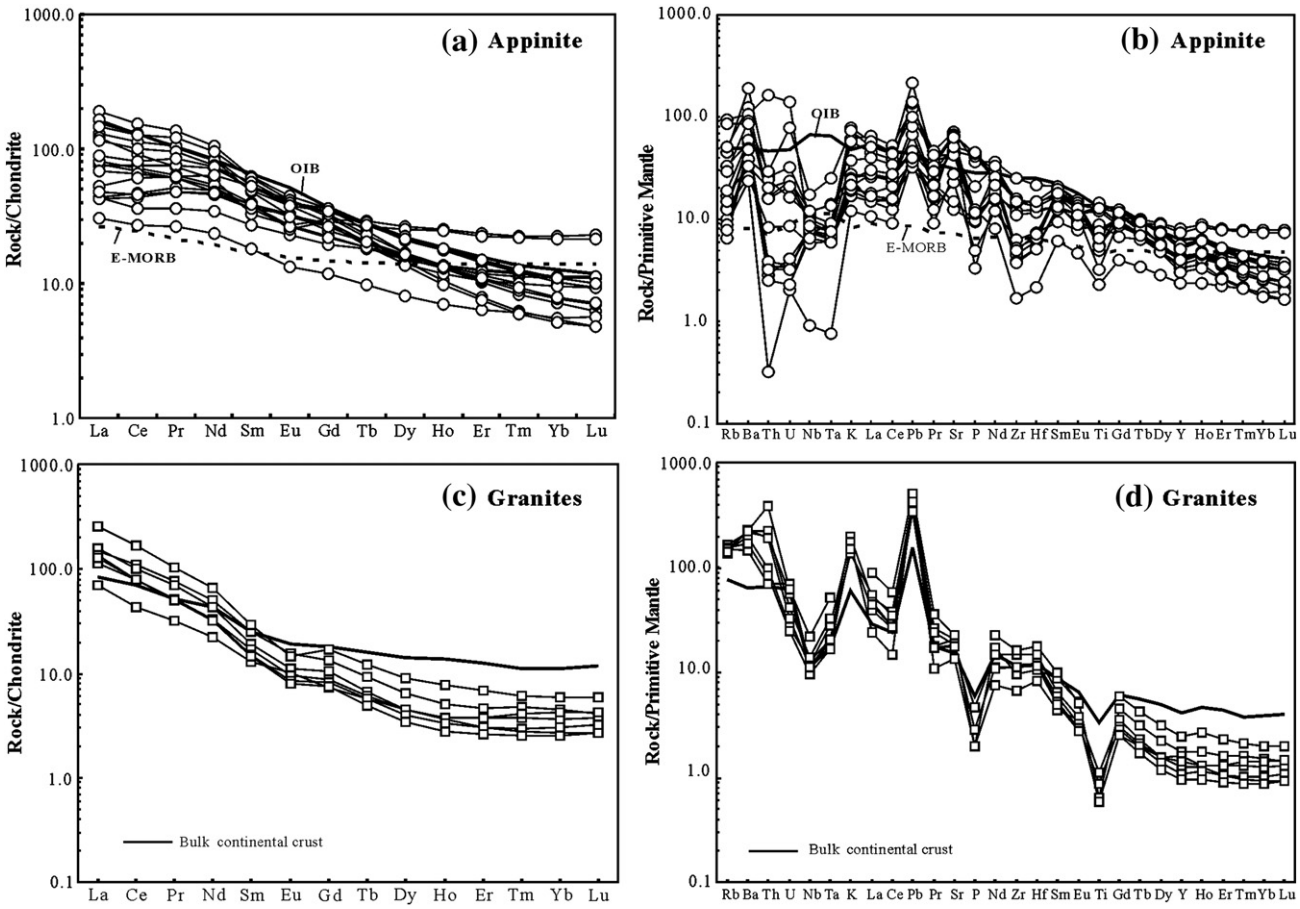

Fig. 5. (a), (c) Chondrite-normalized REE patterns and. (b), (d) Primitive mantle-normalized trace element spidergrams for the Late Permian appinite–granite suite from northwestern Liaoning.
Normalization values are from Sun and McDonough (1989). The data for oceanic island basalt (OIB) and enriched mid-ocean ridge basalt (E-MORB) are also from Sun and McDonough (1989). Bulk continental crust data are from Rudnick and Gao (2003).

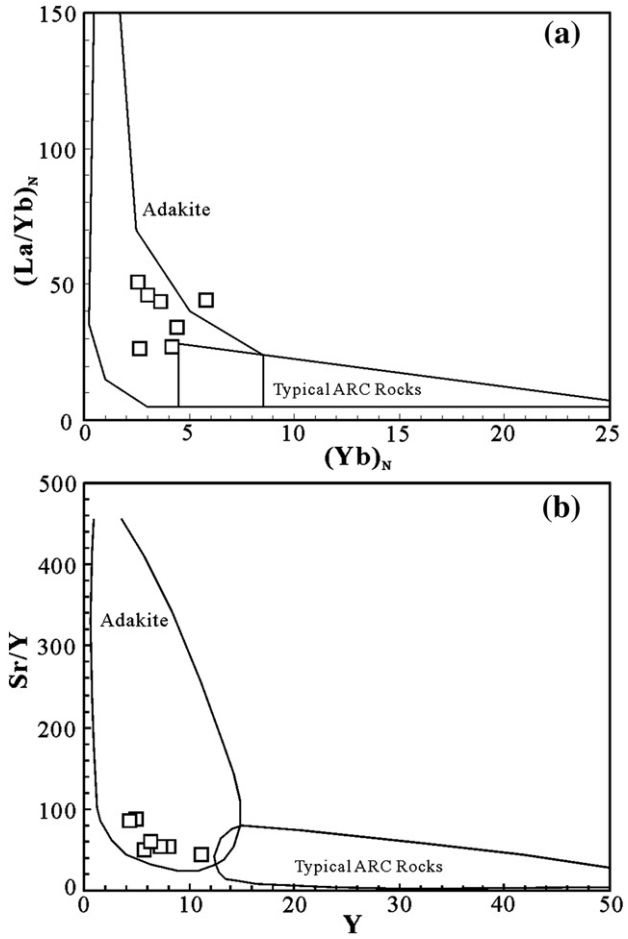

Fig. 6. (a) $(La/Yb)_N$ vs. Yb_N diagram. (b) Sr/Y vs. Y diagram for the Late Permian granite from northwestern Liaoning.
(a) is from Drummond and Defant (1990) and (b) is from Martin (1999).

high-K calc-alkaline character (Fig. 4b) and mainly plot in the alkali-calcic field on the alkali–lime index plot (Fig. 4c), with A/CNK of 1.0 to 1.12 (Fig. 4d) making them peraluminous. In the chondrite-normalized REE diagrams (Fig. 5c), they are enriched in LREE ($La_N/Yb_N = 26.4–43.4$), with minor or no Eu anomalies ($Eu/Eu^* = 0.74–1$; Table 1) and depleted in HREE and Y. In the PM-normalized trace element diagram (Fig. 5d), they show enrichment in LILE and LREE and strong depletion in HFSE. High concentrations of Sr and La and low contents of Y and Yb result in high Sr/Y and La/Yb ratios, and so the samples exclusively fall within the adakite field on $(La/Yb)_N$–Yb_N and Sr/Y–Y diagrams (Fig. 6).

5.3. Whole rock Sr–Nd and zircon Hf isotopes

Table 2 presents the whole-rock Sr–Nd isotope data and the calculated initial Sr–Nd isotopic compositions for the mafic–felsic suite from northwestern Liaoning. As shown in a plot of $\varepsilon_{Nd}(t)$ vs. $^{87}Sr/^{86}Sr_i$ (Fig. 7a), the mafic rocks have initial $^{87}Sr/^{86}Sr$ ratios from 0.7066 to 0.7128 and moderately negative $\varepsilon_{Nd}(t)$ values of −8.3 to −13.3. The diorite sample exhibits an initial $^{87}Sr/^{86}Sr$ ratio of 0.7053, $\varepsilon_{Nd}(t)$ of −17.2 and model age of 2.4 Ga. The granites have initial $^{87}Sr/^{86}Sr$ ratios from 0.7063 to 0.7066, negative $\varepsilon_{Nd}(t)$ values of −15.6 to −16.3 and model ages of 2.2 to 2.3 Ga.

Online Supplemental Table 2 presents the zircon Hf isotope data for the mafic–felsic suite from northwestern Liaoning. Zircons from sample FX06-18 show a range of initial $^{176}Hf/^{177}Hf$ ratios from 0.28209 to 0.28223 and $\varepsilon_{Hf}(t)$ values from −13.8 to −18.7 (Fig. 7b and c), with crustal model ages (T_{DM}^{C}) of 2.15 to 2.45 Ga. Zircons from sample FX06-21 exhibit a range of initial $^{176}Hf/^{177}Hf$ ratios from 0.28203 to 0.28220, $\varepsilon_{Hf}(t)$ from −14.7 to −20.8 (Fig. 7b and c) and crustal model ages between 2.21 and 2.59 Ga. Zircons from sample FX06-52 display a range of initial $^{176}Hf/^{177}Hf$ ratios from 0.28222 to 0.28233, $\varepsilon_{Hf}(t)$ from −15.5 to −18.9 (Fig. 7b and c) and model ages from 1.92 to 2.15 Ga. Zircons from sample FX06-59 have a range of initial $^{176}Hf/^{177}Hf$ ratios from 0.28214 to 0.28223, $\varepsilon_{Hf}(t)$ from −13.5 to −16.8 (Fig. 7b and c) and crustal model ages from 2.13 to 2.34 Ga.

6. Discussion

6.1. Origin of appinitic rocks

With their hornblende-dominated mafic mineral character and calc-alkaline geochemical affinity, the mafic rocks are reminiscent of the so-called appinite suite from various European Caledonian and Variscan batholiths (Atherton and Ghani, 2002; Ayrton, 1991; Bowes and Košler, 1993; Castro et al., 2003; Fowler and Henney, 1996; Fowler et al., 2001, 2008) and low-silica members from some sanukitoid suites worldwide (Heilimo et al., 2010; Kamei et al., 2004; Kovalenko et al., 2005; Tatsumi, 2006). However, with its

Table 2
Rb–Sr and Sm–Nd isotopic compositions for the Late Permian appinite–granite suite from northwestern Liaoning, North China Craton.

Sample no.	Rb [ppm]	Sr [ppm]	$^{87}Rb/^{86}Sr$	$^{87}Sr/^{86}Sr$	(2σ)	$(^{87}Sr/^{86}Sr)_t$	Sm [ppm]	Nd [ppm]	$^{147}Sm/^{144}Nd$	$^{143}Nd/^{144}Nd$	(2σ)	Initial Nd	$\varepsilon_{Nd}(t)$	T_{DM} (Ma)	T_{DM2} (Ma)
Appinites															
FX06-15	9.524	287.4	0.0959	0.713201	13	0.71285	5.666	24.11	0.1421	0.511907	13	0.511670	−12.49	2632	2031
FX06-18	38.66	1497	0.0747	0.707748	13	0.70748	8.410	42.54	0.1195	0.511827	14	0.511628	−13.32	2133	2102
FX06-19	26.84	1533	0.0507	0.707714	10	0.70753	7.263	38.23	0.1148	0.511863	11	0.511671	−12.46	1977	2034
FX06-20	64.71	893.5	0.2095	0.705415	13	0.70534	6.846	35.75	0.1158	0.511624	13	0.511431	−17.16	2365	2413
FX06-52	50.31	934.7	0.1558	0.707658	11	0.70709	8.840	47.05	0.1136	0.512001	13	0.5118111	−9.73	1745	1813
FX06-54	10.16	562.9	0.0522	0.708553	13	0.70836	3.730	14.61	0.1543	0.512140	13	0.511882	−8.34	2578	1694
FX06-57	25.78	1013	0.0737	0.706881	10	0.70661	7.695	32.91	0.1414	0.511920	11	0.511684	−12.22	2579	2009
FX06-62	7.834	1229	0.0184	0.707016	13	0.70695	5.184	20.51	0.1528	0.512086	12	0.511831	−9.35	2648	1776
FX06-59	11.81	1239	0.0276	0.706834	12	0.70677	8.245	36.09	0.1381	0.511946	12	0.511715	−11.6	2416	1960
FX06-65	7.713	1476	0.0151	0.706946	14	0.70689	5.422	21.86	0.1500	0.512096	14	0.511846	−9.06	2509	1753
Granites															
FX06-21	106.0	313.3	0.9791	0.710122	13	0.70657	1.888	10.46	0.1092	0.511693	13	0.511511	−15.60	2117	2288
FX06-22	91.99	426.6	0.6239	0.708794	11	0.70653	2.910	21.27	0.0827	0.511628	11	0.511490	−16.0	1766	2324
FX06-23	106.7	395.1	0.7816	0.709125	11	0.70629	2.405	15.48	0.0939	0.511634	12	0.511477	−16.25	1924	2343
FX06-74	88.73	381.2	0.6736	0.708957	12	0.70650	2.195	14.86	0.0893	0.511642	15	0.511492	−15.93	1842	2318

Chondrite Uniform Reservoir (CHUR) values ($^{87}Rb/^{86}Sr = 0.0847$, $^{87}Sr/^{86}Sr = 0.7045$, $^{147}Sm/^{144}Nd = 0.1967$, $^{143}Nd/^{144}Nd = 0.512638$) are used for the calculation. $\lambda_{Rb} = 1.42 \times 10^{-11}$ year^{-1} (Steiger and Jäger, 1977); $\lambda_{SM} = 6.54 \times 10^{-12}$ year^{-1} (Lugmair and Marti, 1978).

low-silica contents and variable Mg#, the appinite suite is distinct from typical sanukitoid rocks that commonly have an intermediate silica content (55–70 wt.%) and elevated Mg# (45–65) (Heilimo et al., 2010). Therefore, the likelihood is that both suites seem to constitute complementary members of a continuous magmatic spectrum with a similar origin. Given silica contents lower than 55% in most samples, the present mafic rocks mainly belong to the appinite suite.

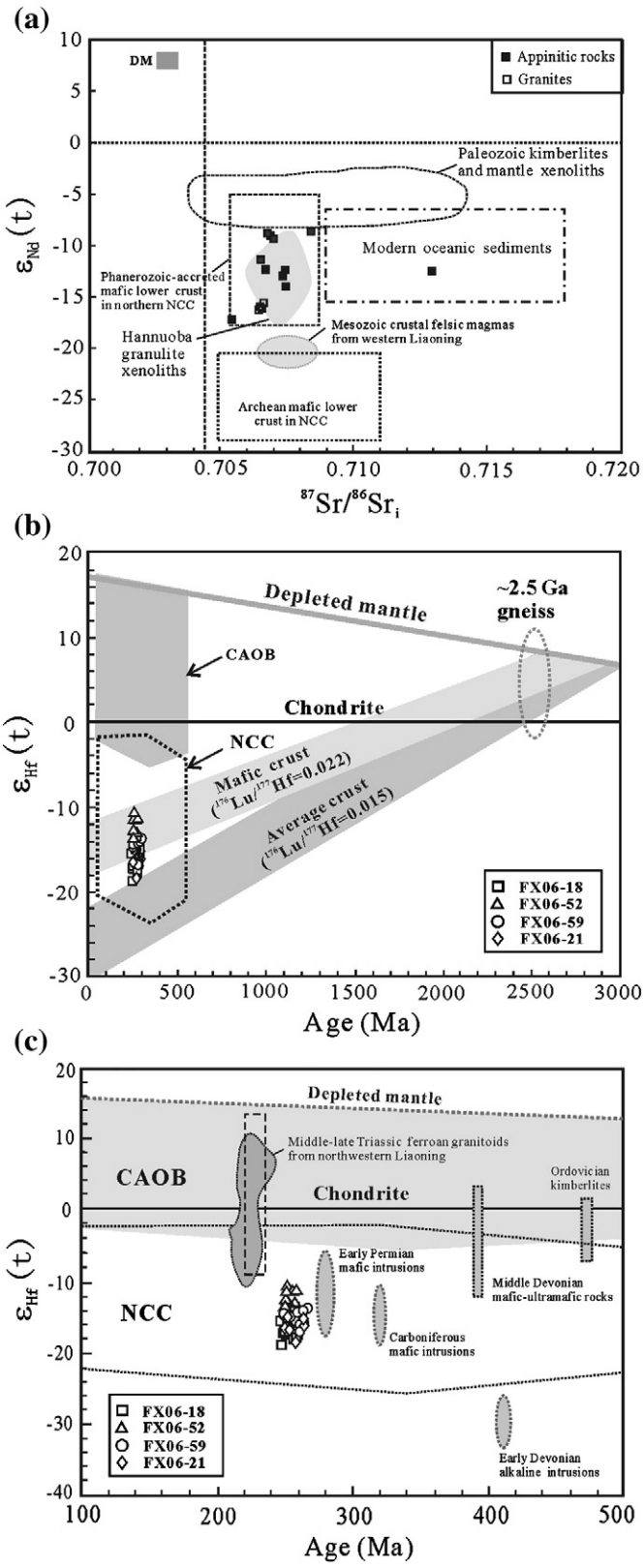

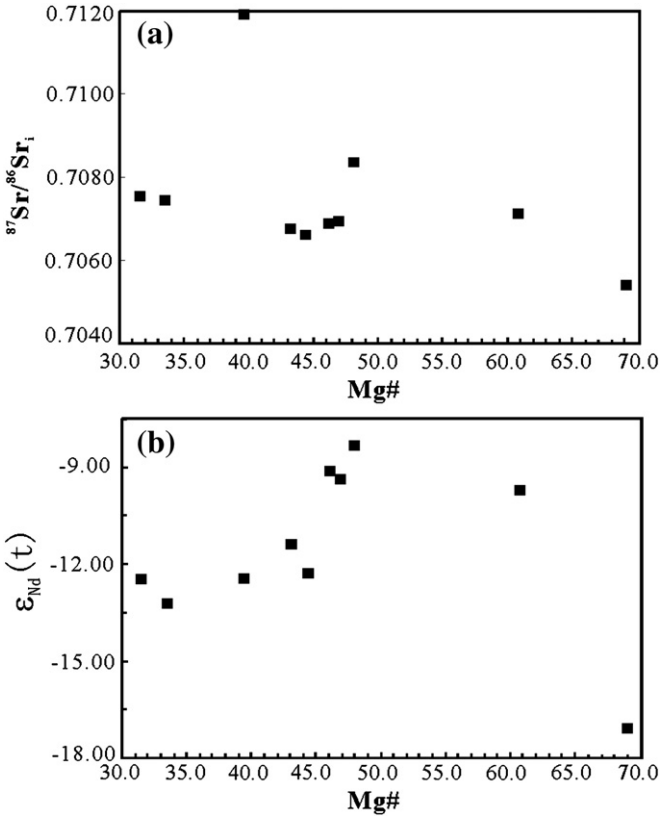

Fig. 8. Plots of (a) $^{87}Sr/^{86}Sr_i$ vs Mg# and (b) $\varepsilon_{Nd}(t)$ vs. Mg# for the Late Permian appinite suite from northwestern Liaoning.

By analogy, such petrologic and geochemical features (low silica and high MgO contents) are distinct from those of any crustal materials (Rudnick and Gao, 2003) or crust-derived melts (e.g., Patiño Douce and Beard, 1995; Patiño Douce and McCarthy, 1997) but reflect a mantle derivation. This is consistent with the subduction-related metasomatized mantle parentage commonly envisioned for appinitic (Fowler and Henney, 1996; Fowler et al., 2001, 2008; Ye et al., 2008; X.H. Zhang et al., 2012a) and sanukitoid suites (Heilimo et al., 2010; Kamei et al., 2004; Kovalenko et al., 2005).

Like other hornblende-rich mafic to ultramafic intrusions (Fowler and Henney, 1996; Fowler et al., 2001, 2008; Roberts et al., 2000), a complex liquid-crystal process may be involved in the petrogenesis of these mafic rocks. On one hand, their field occurrence as wide dikes seems to mitigate against a cumulate origin. Their moderate MgO, Cr and Ni contents is also far below those expected for the rocks with a cumulate origin (MgO > 15%, Cr > 2000 ppm, Ni > 300 ppm) (Roberts et al., 2000). On the other hand, the moderate Mg# and low transitional

Fig. 7. Plots of (a) $\varepsilon_{Nd}(t)$ vs. $^{87}Sr/^{86}Sr_i$, (b) zircon $\varepsilon_{Hf}(t)$ vs. U–Pb age from 0 to 3000 Ma and (c) zircon $\varepsilon_{Hf}(t)$ vs. U–Pb age from 100 to 500 Ma for the Late Permian appinite–granite suite from northwestern Liaoning.
In (a), The Mesozoic crust-derived felsic magma from western Liaoning is from Zhang et al. (2008b). The field for Paleozoic kimberlites and mantle xenoliths from the eastern NCC is from Wu et al. (2006b). The field for the Hannuoba lower crustal xenoliths is from Zhou et al. (2002). The field for the modern oceanic sediments is from Plank and Langmuir (1998) and Patino et al. (2000). Archean mafic lower crust of the NCC is from Jahn et al. (1987, 1999). In (b), fields for the CAOB and NCC are from Yang et al. (2006). The field for Archean gneiss is from Liu et al. (2011) and Wang et al. (2011). In (c), fields for Ordovician kimberlites, Early Devonian alkaline intrusions, Middle Devonian mafic–ultramafic rocks, Carboniferous, Early Permian mafic intrusions from the northern NCC and Middle to Late Triassic ferroan granitoids from northwestern Liaoning are from Yang et al. (2009), S.H. Zhang et al. (2009a, 2009b), Zhang et al. (2010b, 2011a) and X.H. Zhang et al. (2012a), respectively. Dashed line in (c) area represents detrital zircons from the Xinglonggou formation in northwestern Liaoning (Meng et al., 2010).

metal abundances in some samples indicate that these mafic rocks may have experienced some crystal fractionation, most likely of amphibole, plagioclase, ilmenite and apatite, as reflected by systematic variations of major oxides and compatible trace element with MgO and the Cr–Ni fractionation vector (Online Supplemental Fig. 1). Therefore, it seems that only a few mafic samples maintain a relatively primary affinity to their mantle precursor.

Given their cratonic occurrence, the mafic rocks could have suffered from crustal contamination and this is usually the case for appinitic and sanukitoid magmas emplaced in a continental setting (Castro et al., 2003; Qian and Hermann, 2010). However, they lack any petrographic characters indicative of crustal assimilation, as does the Cretaceous Hanxin sanukitoid suite from the NCC (Qian and Hermann, 2010). In terms of trace elements, the northern Liaoning mafic rocks have much higher Sr (312–1498 ppm) than that of continental crust in general (Rudnick and Gao, 2003) and the local basement country rocks (84–304 ppm) as represented by the Jianping complex (Liu et al., 2011; Wang et al., 2011). Furthermore, the lack of any systematic correlation of $^{87}Sr/^{86}Sr_i$ and $\varepsilon_{Nd}(t)$ with varying MgO in the appinitic rocks is inconsistent with the trend commonly expected in simple cases of progressive crustal contamination (Fig. 8).

Following the argument that parental melts from mantle sources can be potentially identified using the relative Mg# of mafic rocks (e.g., McMillan et al., 2003), those samples with relatively high Mg# (>60) and Cr (300–617 ppm) abundances are most likely to have a composition closest to primary basaltic melts in terms of elemental and isotopic compositions. As such, variable but consistently unradiogenic Nd isotopic compositions in these samples attest to a highly heterogeneous enriched mantle source.

As is implied in various petrogenetic models for appinitic and sanukitic magmas, such an enriched mantle source can be ascribed to slab involvement (Fowler, et al., 2001, 2008; Heilimo et al., 2010; Kamei et al., 2004; Kovalenko et al., 2005; Tatsumi, 2006), commonly in the form of variable slab components (altered oceanic crust, sediments or both) and different transfer mechanisms (as a fluid or melt, or both). These metasomatic agents of subduction affinity tend to produce distinctive trace element and isotopic imprints in the metasomatized mantle. For instance, aqueous liquids are thought to be favorable carriers for LILE but not for Th and the LREE (McCulloch and Gamble, 1991; Pearce et al., 1999). Concomitant elemental variations due to the fractionation of selected element pairs (such as Ba/La, Th/La, Sr/Th or Th/Ce) can thereby be taken to monitor potential fluid or sediment contributions to magma source regions (Turner et al., 2012; Woodhead, et al., 2001). In the current case, high Ba/La and Th/Ta ratios in the mafic rocks may reflect potential dual inputs of slab-derived fluids and sediment-released hydrous melts (Fig. 9a), while the curved array extending from high Sr/Th at low Th/Ce and elevated Th/Ce at low Sr/Th also indicates contributions from an aqueous fluid component and a sediment melt (Turner et al., 2012) (Fig. 9b).

Such duality is perfectly compatible with the complex nature of subducted sediments, including such diverse solid components as terrigenous sediments, pelagic clays and chemical precipitates (Fe–Mn crusts) (e.g., Marini et al., 2005; Plank and Langmuir, 1998), and also various fluid derivatives (Kessel et al., 2005; Portnyagin et al., 2007; Schmidt et al., 2004). Variable solid components tend to exhibit distinct REE and HFSE signatures corresponding to their different behaviors during sedimentary processes (Altherr et al., 2004; Marini et al., 2005). Terrigenous sediments commonly have higher ratios of Hf/Sm and Hf/Nd and lower Lu/Hf ratio than pelagic clays and chemical precipitates. The attendant isotopic variation is a non-radiogenic signature for the former and more radiogenic one for the latter. On the other hand, liquid/sediment-derivatives can be present in the form of aqueous fluids, melts or supercritical liquids depending on temperatures and pressures (Kessel et al., 2005). Several

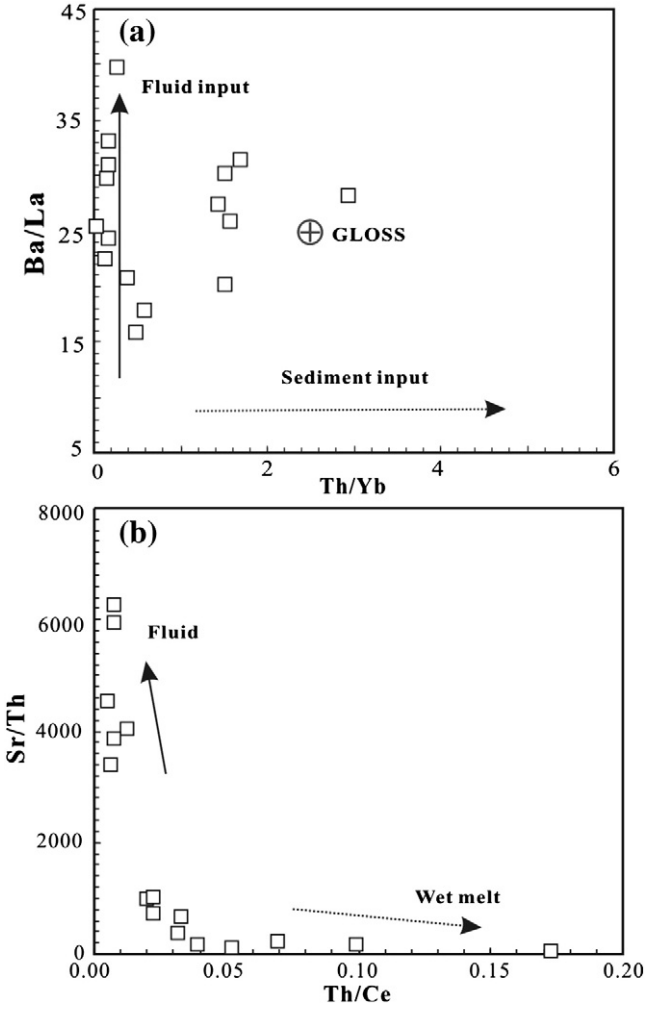

Fig. 9. (a) Ba/La vs. Th/Yb and (b) Sr/Th vs. Th/Ce plots for the Late Permian appinite suite from northwestern Liaoning.
In (a), continuous vector, slab-derived fluids; dashed vector, sediment input in the source as represented and discussed by Woodhead et al. (2001). Global subducting sediment (GLOSS) compositions are from Plank and Langmuir (1998).

experimental and geochemical studies (Kessel et al., 2005; Portnyagin et al., 2007; Schmidt et al., 2004) suggest that such melts and liquids show contrasting behavior of U, Th, Sr, Ba, Be and LREE with varying temperatures at shallow depths, whereas solute-rich supercritical liquids could be effective agents for removing a large fraction of Rb, Sr, Ba, LREE, Pb, Th and U from the sediments (Kessel et al., 2005; Schmidt et al., 2004). Specifically, Sr is not carried into the mantle by low-density fluids at T<900 °C, but is efficiently transported in the higher-T, low density fluids, melts and high-density fluids, with a partition coefficient of about 20 (Clemens et al., 2009).

With these complicated effects from variable coupling between somewhat heterogeneous terrigenous–hemipelagic components and different carrier agents, the observed elemental variations and coupled radiogenic Sr but unradiogenic Nd–Hf isotopic signatures in the appinitic rocks can be properly accounted for. Specifically, elevated Hf/Sm and low Nd/Hf ratios in some samples may reflect the involvement of a terrigenous component with detrital zircon, whereas the large negative Zr–Hf anomalies in others (e.g., FX06-58) can be attributed to the presence of residual zircon. High Ba/Th and Ba/La in some samples could result from certain amounts of a Ba-enriched sedimentary component, such as pelagic clays, whereas high Sr/Nd ratios may reflect a significant contribution of carbonate components in the subducted sediment. Contrasting concentration of Th and U in

different samples may hinge on the nature of the dominant mobile phases.

6.2. Granite genesis

With their high alkali content, low CaO and P_2O_5, elevated Ba–Sr and low abundances of Nb and Ta, the granites from northern Liaoning show typical features of undifferentiated calc-alkaline I-type felsic magmas (Barbarin, 1999; Landenberger and Collins, 1996). However, high contents of Sr and Ba and high ratios of Sr/Y and La_N/Yb_N (Fig. 6) in the granites bestow a high-silica adakitic affinity on them.

Such adakitic felsic magmas can be attributed to multiple petrogenetic scenarios (Moyen, 2009), including (1) partial melting of subducted oceanic crust and subsequent interaction of the melts with the overlying mantle wedge (Defant and Drummond, 1990); (2) assimilation and fractional crystallization (AFC) involving a mantle-derived basaltic magma (Castillo et al., 1999; Macpherson et al., 2006); (3) partial melting of a high Sr/Y (and La/Yb) source like mafic lower arc crust (Rapp et al., 2002, 2003; Xiao and Clemens, 2006) or mafic lower continental crust (Jiang et al., 2007).

For the granites in this study, their moderately evolved Sr–Nd–Hf_{Zircon} isotopic compositions preclude the possibility of slab melting in conjunction with melt–peridotite interaction. Numerous experimental works also failed to produce any potassic, high-silica melts from MORB-like compositions (López and Castro, 2001; Rapp and Watson, 1995).

With the coexistence of coeval mafic rocks, the granites herein could have been produced by an AFC process from these progenitor mafic magmas. However, the odds are against this possibility. First, with plagioclase as a liquidus phase in the granites as indicated by the petrography, any prior crystal fractionation would have considerably increased Ca/Sr and Rb/Sr ratios. Most current granite samples turned out to have Ca/Sr ratios of 17 to 24, Rb/Sr ratios of 0.23 to 0.32, Rb/Ba ratios of 0.07 to 0.09, and K/Ba ratios of 25 to 43, respectively. These ratios are comparable to those of parental magmas for typical I-type granites (Landenberger and Collins, 1996; Zhang et al., 2011b), and negate any significant prior fractionation of plagioclase. Second, the granitic melts resulting from differentiation should be characterized by strong enrichment in many HFSE, and by consistent chondrite-normalized REE patterns with a concave shape and large negative Eu anomalies. The chemistry of the present granites contrasts markedly with these trends. Third, the granite samples have lower initial $^{87}Sr/^{86}Sr$ ratios than most mafic rocks. This appears to be inconsistent with what might be expected in the case of an AFC process.

These facts lead us to favor a partial melting scenario of high-K mafic lower crust to accommodate geochemical characteristics of current adakitic granites, as advocated by a number of experimental (e.g. Rapp et al., 2002; Sisson et al., 2005; Xiao and Clemens, 2006) and geochemical case studies (Jiang et al., 2007; Zhang et al., 2011a). With their evolved whole-rock Sr–Nd and zircon Hf isotopic compositions ($^{87}Sr/^{86}Sr_i = 0.7062$ to 0.7066, $\varepsilon_{Nd}(t) = -15.6$ to -16.3, zircon $\varepsilon_{Hf}(t) = -14.7$ to -20.8), these granites not only overlap the coeval appinitic and intermediate rocks (Fig. 7), but also locate towards a pure Archean lower crust-derived felsic magma as represented by the Jurassic Lüshan granite from western Liaoning (Zhang et al., 2008b) and ancient crustal ingredients involved in the Cretaceous alkaline rocks from the northern NCC (Yang et al., 2008b). Moreover, these isotopic variations resemble those of Phanerozoic newly-accreted mafic lower crust from the northern NCC (Fig. 7a), which is constrained by episodic magma underplating as represented by multiple Late Paleozoic mafic–ultramafic intrusions (Chen et al., 2009; S.H. Zhang et al., 2009a, 2009b; Zhang et al., 2011a; X.H. Zhang et al., 2012a) and granulite xenoliths (Liu et al., 2004; H.F. Zhang et al., 2012a; Zhou et al., 2002). This isotopic similarity, in conjunction with the confined field occurrence of the granites into the appinitic rocks, leads us to the inference that these granites were produced

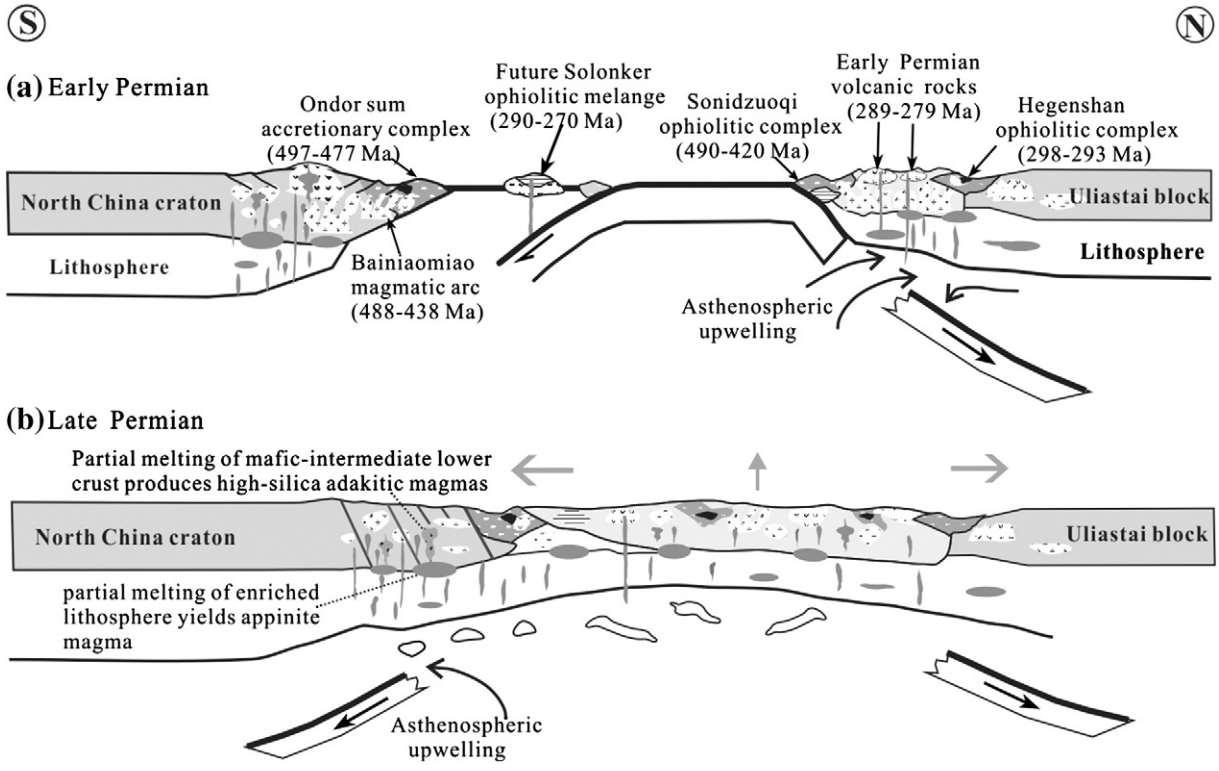

Fig. 10. Simplified cross-sections to illustrate the tectonic evolution in northern China in the Permian. (a) Early Permian; (b) Late Permian. (a) is modified after Zhang et al. (2011a), and (b) is modified after Zhang and Zhai (2010).

by melting of a mixed lithology containing a dominant newly underplated mafic lower crustal component and a minor amount of ancient mafic lower crust.

6.3. Tectonic implications

The well-defined ages presented herein established an emplacement time of Late Permian for the Hercynian appinite–granite complex in northwestern Liaoning. Of special note about the ages is that sample FX06-59, which was collected from an iron ore quarry in the Ahalai dioritic unit, was previously regarded to be part of the Proterozoic Jiumiao dioritic batholith (LBGMR, 1971, 1996). This revelation, plus the similarity in mineralogical constituents and petrological character between the Ahalai unit and the main part of the Jiumiao pluton, raises the possibility that the Jiumiao dioritic batholith might not be Proterozoic. Clearly, further work is needed to constrain the proper affiliation of this important intrusive complex.

Late Paleozoic paleogeographic and paleotectonic reconstructions of the northern China–Mongolia tract indicate that final closure of the Paleo-Asian Ocean happened along the Solonker suture zone between the northern and southern continental blocks (Jian et al., 2010; Windley et al., 2007; Xiao et al., 2003). The most highlighted but ongoing controversial issues concerning this zone are determining its final suturing time and the evolved tectonic affinity of the opposite-facing continental blocks (the Uliastai Block and the NCC). Some authors suggest that final suturing took place during the latest Permian to Early Triassic (Chen et al., 2000; Xiao et al., 2003), whereas others advocate a timing of Late Devonian to Early Carboniferous (Hong et al., 1995; Shao, 1991) or Early Permian (Zhang et al., 2008a). Jian et al. (2010) recently proposed an intraoceanic arc-trench system above a south-dipping subduction zone through a geochronological and geochemical study of the ophiolitic rocks from the Solonker zone. This resulted in identification of a sequence of Permian tectonic–magmatic events during the life cycle of a supra-subduction zone-type ophiolite, including pre-subduction (c. 299–290 Ma), subduction initiation (c. 294–280 Ma), ridge-trench collision (c. 281–273 Ma) and post-collisional phase (c. 260–248 Ma) (Jian et al., 2010). Noting the coincidence between the north-dipping slab-breakoff beneath the northern continental block and the south-dipping intra-oceanic subduction initiation, we further argue that it is the former that led to the switch in subduction polarity in the Solonker zone and initiated the south-dipping subduction as recorded by the Solonker ophiolite (Fig. 10a) (Zhang et al., 2011b). Given its short life cycle (<30 Ma), the Solonker ophiolitic complex, as defined by Jian et al. (2010), may be compatible with the time scale of restricted oceanic plates that could exist during a post-collisional stage in the paradigm of an orogenic cycle (Bonin, 2004; Liégeois, 1998; Zhang et al., 2011a). Moreover, the distinctive scenario of growth-dominated crustal evolution in the north versus a reworking-oriented one in the south fits well with two contrasting Phanerozoic orogenic systems recorded by zircon hafnium isotope data from orogens worldwide since 550 Myr ago (Collins et al., 2011). Superimposed on the predominantly N-directed subduction is short-term, localized S-dipping subduction possibly triggered by intermittent slab flipping during closure of backarc basins (Collins et al., 2011).

Therefore, it follows that a post-orogenic extensional regime has prevailed in the northern NCC from Late Permian onward. This is evidenced by the widespread occurrence of Late Permian to Middle Triassic post-orogenic magmatic rocks along the western segment of the northern NCC (Fu et al., 2012; S.H. Zhang et al., 2009a, 2009b) and in adjacent regions of the CAOB (Wu et al., 2011; X.H. Zhang et al., 2009; Zhang et al., 2010b). The appinite–granite complexes, with their dual source regions of metasomatized lithospheric mantle and mixed lower crust, are typical for post-collisional/orogenic calc-alkaline mafic–felsic igneous suites (Bonin, 2004). These magma sources are commonly the result of asthenospheric upwelling following lithospheric delamination during a post-subduction extensional regime, as in the case of the appinite–granite associations from the British Caledonides (Atherton and Ghani, 2002) and the Silurian to Devonian magmatism in the Tibet Plateau (Ye et al., 2008). This leads to basaltic underplating and the attendant underplated magmas may have provided the heat necessary for melting of the mafic to intermediate lower crustal rocks to produce high-K felsic magmas (Fig. 10b).

As in the case of their Carboniferous predecessors (X.H. Zhang et al., 2012a), it is not easy to determine the exact metasomatic timing in the present appinites, given the documentation of multiple subduction-related metasomatic events in the northern NCC, like the Neo-Archean (~2.5 Ga) subduction along an active continental margin (Liu et al., 2011; Wang et al., 2011), Paleoproterozoic (~1.85 Ga) subduction/collision between the Eastern and Western Blocks (Wang et al., 2006; Zhao et al., 2001), ~1.35 Ga diabase intrusive that coincided with the Hf model age in the baddeleyites from the Ordovician kimberlites (Li et al., 2011) and Early Paleozoic subduction that led to the Devonian amalgamation between the NCC and the Bainaimiao arc terrane (Zhang et al., 2010a). The most likelihood is that the formation of these appinites might have involved a distinct two-stage process: (1) a precursor metasomatic stage of mantle peridotite enriched by melts and fluids from subducted sediments and (2) a delayed partial melting stage of metasomatized mantle by a thermal event long after subduction. It is the protracted elapse between two stages that might bequeath a highly enriched isotopic signature to the mantle source, analogous to the situation of numerous Late Archean sanukitoids (Heilimo et al., 2010; Kovalenko et al., 2005; Whalen et al., 2004) and Mesozoic high-Mg diorites from the NCC (Wang et al., 2006).

With an age of Late Permian, the appinite–granite suite in northern Liaoning appears to be coincident with the main activity of the EW-trending fault system along the northern margin of the NCC, which is constrained by a series of mineral $^{40}Ar/^{39}Ar$ ages from 260 to 249 Ma for mylonites from different faults in the area (Hu et al., 2003; Wan, 2012; Zhang et al., 2005). These ages, together with the related structural signatures of dextral transcurrent movements (Wan, 2012; Zhang et al., 2001, 2005), indicate that the northern NCC might be under a transcurrent regime during the Late Permian following amalgamation between the NCC and terranes of the CAOB (Cui et al., 2002; Hu et al., 2003; Wan, 2012; Zhang et al., 2005). Therefore, this corroborates the long-noted spatial and temporal connection between magmatic activity and transcurrent movements on these controlling faults (Cui et al., 2002; S.H. Zhang et al., 2009b; Zhang et al., 2010b). Such an intimate relationship is strikingly similar to that in the British Caledonides (Brown et al., 2008; Fowler and Henney, 1996; Hutton and Reavy, 1992; Rogers and Dunning, 1991) and the European Variscan belt (Słaby et al., 2010), where the ages of appinitic and related granitic rocks have been used to constrain the timing of transcurrent movements on the major controlling faults (Hutton and Reavy, 1992; Rogers and Dunning, 1991). Collectively, these specific Asian and European case examples testify to a general characteristic of temporal and spatial linkage of post-orogenic magmatism with large-scale horizontal movements along major shear zones (e.g., Bonin, 2004; Liégeois, 1998). As in the case of the British Caledonian situation, such lithospheric-scale transcurrent faults not only facilitated the genesis of mantle-derived appinitic and lower-crustal-derived felsic magmas along the northern NCC, but also provided a favorable plumbing system for the ascent and emplacement of these magmas.

The present appinitic rocks, along with other episodes of Late Paleozoic to Mesozoic amphibole-rich mafic to intermediate intrusions in the NCC (Chen et al., 2009; Qian and Hermann, 2010; Wang et al., 2006; S.H. Zhang et al., 2009b; X.H. Zhang et al., 2012a), may constitute an extensive newly-accreted enriched underplate within the middle–lower crust of the craton, echoing episodic

Phanerozoic growth and modification of the Precambrian lower crust beneath the NCC (H.F. Zhang et al., 2012a, 2012b). This is reminiscent of the British Caledonides, where such underplates played an essential role in the formation of some high-Ba–Sr granites. Nevertheless, the present case takes a distinctive flavor from the differentiation model of Fowler et al. (2001) with reference to the Caledonian granitoids. The latter implies that high-Ba–Sr granites could evolve from contemporaneous appinitic magmas by protracted fractional crystallization and represent production of juvenile continental crust in the Phanerozoic. Instead, our case study resembles the model of Neilson et al. (2009) and exemplifies a crustal anatexis model that involves progenitor basaltic extraction, resultant magmatic underplating, lower crustal anatexis and subsequent magma fractionation (Fig. 10b), likely in response to delamination during the final closure of the Paleo-Asian Ocean. This indicates that both mechanisms can convert basic crust into a felsic one and thus control the chemical differentiation of the continental crust (Kemp and Hawkesworth, 2003). In contrast to voluminous Phanerozoic crustal growth in the British Caledonian case, the NCC case documents little juvenile crustal addition but reworking during most of the Paleozoic. It was not until the Early to Middle Triassic that ushered in a growth (juvenile crustal addition)-oriented decratonization stage, as evidenced by the Xinglonggou volcano-sedimentary formation (Meng et al., 2010) and the Middle to Late Triassic ferroan granitoids of northwestern Liaoning (X.H. Zhang et al., 2012b) (Fig. 7c).

7. Conclusions

SHRIMP and LA-ICP-MS zircon U–Pb dating constrains the emplacement time for the Hercynian appinite–granite complex in northwestern Liaoning along the northern margin of the NCC to the Late Permian. Geochemical and isotopic tracing indicates that the hornblende-rich appinitic rocks were likely derived from partial melting of a subduction-related metasomatized lithospheric mantle, while the adakitic granites were formed through partial melting of mixed protoliths composed of predominant newly-underplated mafic lower crust and minor ancient crustal materials. This peculiar mafic/felsic magmatic coupling leads to three geological implications: (a) it attests to a heterogeneously enriched sub-continental lithospheric mantle along the northern edge of the NCC, (b) it relates to a major post-subduction transcurrent fault along the craton–orogen boundary, and (3) it records reworking within a post-orogenic transcurrent regime associated with lithospheric delamination.

Supplementary data to this article can be found online at http://dx.doi.org/10.1016/j.lithos.2012.09.002.

Acknowledgments

We thank H. Li and X.D. Jin for their help in major and trace element analysis; C.F. Li for Sr–Nd isotope analysis, H.H. Chen for LA-MC-ICP-MS U–Pb dating and Y.B. Zhang for LA-MC-ICP-MS Hf isotopic determinations. Special thanks are also due to Dr. E. Heilimo, Prof. Nelson Eby and an anonymous reviewer for their constructive comments. This study was financially supported by the Major State Basic Research Program of the People's Republic of China (grant no. 2012CB416603), the National Natural Science Foundation of China (grant nos. 90914008), the Knowledge Innovation Program of the Chinese Academy of Sciences (grant no. KZCX2-YW-QN115) and the NNSFC grant no. 41173043. This is The Institute for Geoscience Research (TIGeR) publication no. 426.

References

Altherr, R., Meyer, H.P., Holl, A., Volker, F., Alibert, C., McCulloch, M.T., Majer, V., 2004. Geochemical and Sr–Nd–Pb isotopic characteristics of Late Cenozoic leucite lamproites from the East European alpine belt (Macedonia and Yugoslavia). Contributions to Mineralogy and Petrology 147, 58–73.

Anderson, T., 2002. Corrections of common lead in U–Pb analyses that do not report ^{204}Pb. Chemical Geology 192, 59–79.

Atherton, M.P., Ghani, A.A., 2002. Slab breakoff: a model for Caledonian, Late Granite syn-collisional magmatism in the orthotectonic (metamorphic) zone of Scotland and Donegal, Ireland. Lithos 62, 65–85.

Ayrton, S.N., 1991. Appinites, lamprophyres and mafic magmatic enclaves: three related products of interaction between acid and mafic magmas. In: Didier, J., Barbarin, B. (Eds.), Enclaves and Granite Petrology. : Developments in Petrology. Elsevier, Amsterdam, pp. 465–478.

Bailey, E.B., Maufe, H.B., 1916. The geology of Ben Nevis and Glen Coe and the surrounding country. Memoirs of the Geological Survey of Scotland: Edinburgh. 247.

Barbarin, B., 1999. A review of the relationships between granitoid types, origins and their geodynamic environments. Lithos 46, 605–626.

Bea, F., Montero, P., Molina, J.F., 1999. Mafic precursors, peraluminous granitoids, and lamprophyres in the Avila batholith: a model for the generation of Variscan batholiths in the Iberia. Journal of Geology 107, 399–419.

Bonin, B., 2004. Do coeval mafic and felsic magmas in post-collisional to within-plate regimes necessarily imply two contrasting, mantle and crustal, sources? A review. Lithos 78, 1–24.

Bowes, D.R., Košler, J., 1993. Geochemical comparisons of the subvolcanic appinite suites of the British Caledonides and the Durbachite suite of the central European Hercynides: evidence for associated shoshonitic and granitic magmatism. Mineralogy and Petrology 48, 47–63.

Brown, P.E., Ryan, P.D., Soper, N.J., Woodcock, N.H., 2008. The newer granite problem revisited: a transtensional origin for the early Devonian Trans-Suture suite. Geological Magazine 145, 235–256.

Castillo, P.R., Janney, P.E., Solidum, R.U., 1999. Petrology and geochemistry of Camiguin Island, southern Philippines: insights to the source of adakites and other lavas in a complex arc setting. Contributions to Mineralogy and Petrology 134, 33–51.

Castro, A., Corretgé, l.G., De La Rosa, J.D., Fernandez, C., López, S., García-Moreno, O., Chacón, H., 2003. The appinite–migmatite complex of sanabria, NW Iberian Massif, Spain. Journal of Petrology 44, 1309–1344.

Chen, B., Jahn, B.M., Wilde, S., Xu, B., 2000. Two contrasting Paleozoic magmatic belts in northern Inner Mongolia, China: petrogenesis and tectonic implications. Tectonophysics 328, 157–182.

Chen, B., Suzuki, K., Tian, W., Jahn, B.M., Ireland, T., 2009. Geochemistry and Os–Nd–Sr isotopes of the Gaositai Alaskan-type ultramafic complex from the northern North China craton: implications for mantle–crust interaction. Contributions to Mineralogy and Petrology 158, 683–702.

Chi, G.C., Lin, W.F., 1999. Geological characteristics of Chahaershan and Xiaoouliying ultra-unit granites in West Liaoning. Liaoning Geology 16, 288–300.

Clemens, J.D., Darbyshire, D.P.F., Flinders, J., 2009. Sources of post-orogenic calcalkaline magmas: the Arrochar and Garabal Hill-Glen Fyne complexes, Scotland. Lithos 112, 524–542.

Collins, W.J., Belousova, E.A., Kemp, A.I.S., Murphy, B., 2011. Two contrasting Phanerozoic orogenic systems revealed by hafnium isotope data. Nature Geoscience 4, 333–337.

Cui, S.Q., Li, J.R., Wu, Z.H., Yi, M.C., Shen, S.M., Yin, H.R., Ma, Y.S., 2002. Mesozoic and Cenozoic intracontinental orogenesis of the Yanshan area, China. Geological Publishing House, Beijing. 311 pp.

Davis, G.A., Zheng, Y., Wang, C., Darby, B.J., Zhang, C., Gehrels, G.E., 2001. Mesozoic tectonic evolution of the Yanshan fold and thrust belt, with emphasis on Hebei and Liaoning provinces, northern China. In: Hendrix, M.S., Davis, G.A. (Eds.), Paleozoic and Mesozoic Tectonic Evolution of Central and Eastern Asia: From Continental Assembly to Intracontinental Deformation: Geological Society of America Memoir, 194, pp. 171–197.

Defant, M.J., Drummond, M.S., 1990. Derivation of some modern arc magmas by melting of young subducted lithosphere. Nature 347, 662–665.

Drummond, M.S., Defant, M.J., 1990. A model for trondhjemite–tonalite–dacite genesis and crustal growth via slab melting: Archean to modern comparison. Journal of Geophysical Research 95 (B13), 21503–21521.

Fowler, M.B., Henney, P.J., 1996. Mixed Caledonian apinite magmas: implications for lamprophyre fractionation and high Ba–Sr granite genesis. Contributions to Mineralogy and Petrology 126, 199–215.

Fowler, M.B., Henney, P.J., Darbyshire, D.P.F., Greenwood, P.J., 2001. Petrogenesis of high Ba–Sr granites: the Rogart pluton, Sutherland. Journal of the Geological Society of London 158, 521–534.

Fowler, M.B., Kocks, H., Darbyshire, D.P.F., Greenwood, P.B., 2008. Petrogenesis of high Ba–Sr plutons from the Northern Highlands Terrane of the British Caledonian Province. Lithos 105, 129–148.

Frost, B.R., Barnes, C.G., Collins, W.J., Arculus, R.J., Ellis, D.J., Frost, C.D., 2001. A geochemical classification for granitic rocks. Journal of Petrology 42, 2033–2048.

Fu, L., Wei, J., Kusky, T.M., Chen, H., Tan, J., Li, Y., Kong, L., Jiang, Y., 2012. Triassic shoshonitic dykes from the northern North China craton: petrogenesis and geodynamic significance. Geological Magazine 149, 39–55.

Griffin, W.L., Powell, W.J., Pearson, N.J., O'Reilly, S.Y., 2008. GLITTER: data reduction software for laser ablation ICP-MS. In: Sylvester, P. (Ed.), Laser Ablation-ICP-MS in the Earth Sciences: Mineralogical Association of Canada Short Course Series, vol. 40, pp. 204–207. Appendix, 2.

Heilimo, E., Halla, J., Hölttä, P., 2010. Discrimination and origin of the sanukitoid series: geochemical constraints from the Neoarchean western Karelian Province (Finland). Lithos 115, 27–39.

Hong, D.W., Huang, H.Z., Xiao, Y.J., Xu, H.M., Jin, M.Y., 1995. Permian alkaline granites in central Inner Mongolia and their geodynamic significance. Acta Geologica Sinica 8, 27–39.

Hu, L., Song, H.L., Yan, D.P., Hu, D.G., 2003. The $^{40}Ar/^{39}Ar$ geochronology constraint and geological significance of mylonites in Shangyi–Chicheng fault belt on the north of North China Craton. Science in China, Series D: Earth Sciences 46, 1134–1142.
Hutton, D.H.W., Reavy, R.J., 1992. Strike-slip tectonics and granite petrogenesis. Tectonics 11, 960–967.
Irvine, T.N., Barager, W.R.A., 1971. A guide to the chemical classification of the common volcanic rocks. Canadian Journal of Earth Sciences 8, 523–548.
Jahn, B.M., Auvray, B., Cornichet, J., Bai, Y.L., Shen, Q.H., Liu, D.Y., 1987. 3.5 Ga old amphibolites from eastern Hebei province, China: field occurrence, petrology, Sm-Nd isochron age and REE geochemistry. Precambrian Research 34, 311–346.
Jahn, B.M., Wu, F.Y., Lo, C.H., Tsai, C.H., 1999. Crust-mantle interaction induced by deep subduction of the continental crust: geochemical and Sr-Nd isotopic evidence from post-collisional mafic-ultramafic intrusions of the northern Dabie complex, central China. Chemical Geology 157, 119–146.
Jian, P., Liu, D.Y., Kroner, A., Windley, B.F., Shi, Y.R., Zhang, W., Zhang, F.Q., Miao, L.C., Zhang, L., Tomurhuu, D., 2010. Evolution of a Permian intraoceanic arc-trench system in the Solonker suture zone, Central Asian orogenic belt, China and Mongolia. Lithos 118, 169–190.
Jiang, N., Liu, Y.S., Zhou, W.G., Yang, J.H., Zhang, S.Q., 2007. Derivation of Mesozoic adakitic magmas from ancient lower crust in the North China Craton. Geochimica et Cosmochimica Acta 71, 2591–2608.
Kamei, A., Owada, M., Nagao, T., Shiraki, K., 2004. High-Mg diorites derived from sanukitic HMA magmas, Kyushu Island, southwest Japan arc: evidence from clinopyroxene and whole rock compositions. Lithos 75, 359–371.
Kemp, A.I.S., Hawkesworth, C.J., 2003. Granitic perspectives on the generation and secular evolution of the continental crust. In: Rudnick, R.L. (Ed.), Treatise on Geochemistry, the Crust, 3. Elsevier Pergamon, Amsterdam, pp. 349–410.
Kessel, R., Schmidt, M.W., Ulmer, P., Pettke, T., 2005. Trace element signature of subduction-zone fluids, melts and supercritical liquids at 120–180 km depth. Nature 437, 724–727.
Kovalenko, A., Clemens, J.D., Savatenkov, V., 2005. Petrogenetic constraints for the genesis of Archaean sanukitoid suites: geochemistry and isotopic evidence from Karelia, Baltic Shield. Lithos 79, 147–160.
Kusky, T.M., Windley, B.F., Zhai, M.G., 2007. Tectonic evolution of the North China Block: from orogen to craton to orogen. In: Zhai, M.G., Windley, B.F., Kusky, T.M., Meng, Q.R. (Eds.), Mesozoic Sub-continental Lithospheric Thinning under Eastern Asia: Geological Society, London. Special Publication, 280, pp. 1–34.
Landenberger, B., Collins, W.J., 1996. Derivation of A-type granites from a dehydrated charnockitic lower crust: evidence from the Chaelundi complex, Eastern Australia. Journal of Petrology 37, 145–170.
Le Maitre, R.W., 2002. A Classification of Igneous Rocks and a Glossary of Terms: Recommendations of the International Union of Geological Sciences Sub-commision on the Systematics of Igneous Rocks. Blackwell, Oxford.
Leake, B.E., Woolley, A.R., Arps, C.E.S., et al., 1997. Nomenclature of amphiboles: report of the subcommittee on amphiboles of the International Mineralogical Association, Commission on New Minerals and Mineral Names. American Mineralogist 82, 1019–1037.
Li, Q.L., Wu, F.Y., Li, X.H., Qiu, Z.L., Liu, Y., Yang, Y.H., Tang, G.Q., 2011. Precisely dating Paleozoic kimberlites in the North China Craton and Hf isotopic constrains on the evolution of the subcontinental lithospheric mantle. Lithos 126, 127–134.
Liaoning Bureau of Geology and Mineral Resources (LBGMR), 1971. 1:50000 scale geological map of Fuxin, Liaoning Province and the related notes (in Chinese).
Liaoning Bureau of Geology and Mineral Resources (LBGMR), 1996. 1:50000 scale geological maps of the Jiumiao, Shabaotai and Haertao, Liaoning Province and the related notes (in Chinese).
Liégeois, J.P., 1998. Preface — some words on the post-collisional magmatism. Lithos 45, XV–XVII.
Lin, W., 1996. Geological characteristics and genesis of intermediate complex bodies in Wuhuanchi–Tiejianggeleng area, Fuxin. Liaoning Geology 2, 118–126.
Liu, Y.S., Gao, S., Yuan, H.L., Zhou, L., Liu, X.M., Wang, X.C., Hu, Z.C., Wang, L.S., 2004. U–Pb zircon ages and Nd, Sr, and Pb isotopes of lower crustal xenoliths from North China Craton: insights on evolution of lower continental crust. Chemical Geology 211, 87–109.
Liu, Y., Gao, S., Hu, Z., Gao, C., Zong, K., Wang, D., 2010. Continental and oceanic crust recycling-induced melt peridotite interactions in the Trans-North China orogen: U–Pb dating, Hf isotopes and trace elements in zircons of mantle xenoliths. Journal of Petrology 51, 537–571.
Liu, S.W., Santosh, M., Wang, W., Bai, X., Yang, P.T., 2011. Zircon U–Pb chronology of the Jianping Complex: implications for the Precambrian crustal evolution history of the northern margin of North China Craton. Gondwana Research 20, 48–63.
López, S., Castro, A., 2001. Determination of the fluid-absent solidus and supersolidus phase relationships of MORB-derived amphibolites in the range 4–14 kbar. American Mineralogist 86, 1396–1403.
Ludwig, K., 2001. User manual for isoplot/EX (2.49). Berkeley Geochronology Center Special Publication No. 1a. 55 pp.
Lugmair, G.W., Marti, K., 1978. Lunar initial $^{143}Nd/^{144}Nd$: differential evolution of the lunar crust and mantle. Earth and Planetary Science Letters 39, 349–357.
Macpherson, C.G., Dreher, S., Matthew, T., Thirlwall, F., 2006. Adakites without slab melting: high pressure differentiation of island arc magma, Mindanao, the Philippines. Earth and Planetary Science Letters 243, 581–593.
Marini, J.C., Chauvel, C., Maury, R.C., 2005. Hf isotope compositions of northern Luzon arc lavas suggest involvement of pelagic sediments in their source. Contributions to Mineralogy and Petrology 149, 216–232.
Martin, H., 1999. The adakitic magmas: modern analog of Archean granitoids. Lithos 46, 411–429.
McCulloch, M.T., Gamble, J.A., 1991. Geochemical and geodynamical constraints on subduction zone magmatism. Earth and Planetary Science Letters 102, 358–374.
McMillan, A., Harris, N.B.W., Holness, M., Ashwal, L., Kelley, S., Rambeloson, R., 2003. A granite-gabbro complex from Madagascar: constraints on melting of the lower crust. Contributions to Mineralogy and Petrology 145, 585–599.
Meng, F.X., Gao, S., Yuan, H.L., Gong, H., 2010. Permian– Triassic (260–220 Ma) crustal growth of eastern central Asian orogenic belt as revealed by detrital zircon studies. American Journal of Science 310, 364–404.
Menzies, M.A., Fan, W.M., Zhang, M., 1993. Palaeozoic and Cenozoic lithoprobe and the loss of >120 km of Archean lithosphere, Sino-Korean craton, China. In: Prichard, H.M., Alabaster, T., Harris, N.B.W., Neary, C.R. (Eds.), Magmatic Processes and Plate Tectonics: Geological Society London, Special Publication, 76, pp. 71–81.
Moyen, J.F., 2009. High Sr/Y and La/Yb ratios: the meaning of the 'adakitic signature'. Lithos 112, 556–574.
Neilson, J.C., Kokelaar, B.P., Crowley, Q.G., 2009. Timing, relations and cause of plutonic and volcanic activity of the Siluro-Devonian post-collision magmatic episode in the Grampian Terrane, Scotland. Journal of the Geological Society of London 166, 545–561.
Patino, L.C., Carr, M.J., Feigenson, M.D., 2000. Local and regional variations in Central American arc lavas controlled by variations in subducted sediment input. Contributions to Mineralogy and Petrology 138, 265–283.
Patiño Douce, A.E., Beard, J.S., 1995. Dehydration-melting of biotite gneiss and quartz amphibolite from 3 to 15 kbar. Journal of Petrology 36, 707–738.
Patiño Douce, A.E., McCarthy, T.C., 1997. Melting of crustal rocks during continental collision and subduction. In: Hacker, B.R., Liou, J.G. (Eds.), When continents collide: geodynamics and geochemistry of ultrahigh-pressure rocks. Kluwer, Dordrecht, pp. 27–55.
Pearce, J.A., Kempton, P.D., Nowell, G.M., Noble, S.R., 1999. Hf–Nd element and isotope perspective on the nature and provenance of mantle and subduction components in western Pacific arc-basin systems. Journal of Petrology 11, 1579–1611.
Pitcher, W.S., 1997. The Nature and Origin of Granite. Chapman & Hall, Glasgow . 321.
Plank, T., Langmuir, C., 1998. The chemical composition of subducting sediment and its consequences for the crust and mantle. Chemical Geology 145, 325–394.
Portnyagin, M., Hoernle, K., Plechov, P., Mironov, N., Khubunaya, S., 2007. Constraints on mantle melting and composition and nature of slab components in volcanic arcs from volatiles (H_2O, S, Cl, F) and trace elements in melt inclusions from the Kamchatka Arc. Earth and Planetary Science Letters 255, 53–69.
Qian, Q., Hermann, J., 2010. Formation of high-Mg diorites through assimilation of peridotite by monzodiorite magma at crustal depths. Journal of Petrology 51, 1381–1416.
Rapp, R.P., Watson, E.B., 1995. Dehydration melting of metabasalt at 8–32 kbar: implications for continental growth and crust–mantle recycling. Journal of Petrology 36, 891–931.
Rapp, R.P., Xiao, L., Shimizu, N., 2002. Experimental constraints on the origin of potassium-rich adakites in eastern China. Acta Petrologica Sinica 18, 293–311.
Rapp, R.P., Shimizu, N., Norman, M.D., 2003. Growth of early continental crust by partial melting of eclogite. Nature 425, 605–609.
Roberts, M.P., Pin, C., Clemens, J.D., Paquette, J., 2000. Petrogenesis of mafic to felsic plutonic rock associations: the Calc-alkaline Quérigut complex, French Pyrenees. Journal of Petrology 41, 809–844.
Rogers, G., Dunning, G.R., 1991. Geochronology of appinitic and related granitic magmatism in the W highlands of Scotland: constraints on the timing of transcurrent fault movement. Journal of the Geological Society of London 148, 17–27.
Rudnick, R.L., Gao, S., 2003. Composition of the continental crust. In: Rudnick, R.L. (Ed.), The Crust, Treatise in Geochemistry, vol. 3. Elsevier-Pergamon, Oxford, pp. 1–64.
Schmidt, M.W., Vielzeuf, D., Auzanneau, E., 2004. Melting and dissolution of subducting crust at high pressures: the key role of white mica. Earth and Planetary Science Letters 228, 65–84.
Shao, J., 1991. Crust Evolution in the Middle Part of the Northern Margin of Sino-Korean Plate. Publishing House of Peking University, Beijing.
Sisson, T.W., Ratajesti, K., Hankins, W.B., Glazner, A.F., 2005. Voluminous granitic magmas from common basaltic sources. Contributions to Mineralogy and Petrology 148, 635–661.
Słaby, E., Breitkreuz, C., Żaba, J., Domańska-Siuda, J., Gaidzik, K., Falenty, K., Falenty, A., 2010. Magma generation in an alternating transtensional–transpressional regime, the Krakow–Lubliniec fault zone, Poland. Lithos 119, 251–268.
Steiger, R.H., Jäger, E., 1977. Subcommission on geochronology; convention on the use of decay constants in geochronology and cosmochronology. Earth and Planetary Science Letters 36, 359–362.
Sun, S.S., McDonough, W.F., 1989. Chemical and isotopic systematics of oceanic basalts: implications for mantle composition and processes. In: Saunders, A.D., Norry, M.J. (Eds.), Magmatism in the Ocean Basins: Geological Society, London, Special Publications, 42, pp. 314–353.
Tatsumi, Y., 2006. High-Mg andesites in the Setouchi volcanic belt, southwestern Japan: analogy to Archean magmatism and continental crust formation? Annual Review of Earth and Planetary Science 34, 467–499.
Turner, S., Caulfield, J., Turner, M., Keken, P., Maury, R., Sandiford, M., Prouteau, G., 2012. Recent contribution of sediments and fluids to the mantle's volatile budget. Nature Geoscience 5, 50–54.
Wan, J.L., 2012. Deformation and geochronology of the Fengning–Longhua fault zone in Yanshan intraplate belt, North China. PhD dissertation. Institute of Geology and Geophysics, Chinese Academy of Sciences. p. 88.
Wang, Y.J., Fan, W.M., Zhang, H.F., Peng, T.P., 2006. Early Cretaceous gabbroic rocks from the Taihang Mountains: implications for a paleosubduction-related lithospheric mantle beneath the central North China Craton. Lithos 86, 281–302.
Wang, W., Liu, S.W., Bai, X., Yang, P., Li, Q., Zhang, L., 2011. Geochemistry and zircon U–Pb–Hf isotopic systematics of the Neoarchean Yixian–Fuxin greenstone belt,

northern margin of the North China Craton: implications for petrogenesis and tectonic setting. Gondwana Research 20, 64–81.
Whalen, J.B., Percival, J.A., McNicoll, V.J., Longstaffe, F.J., 2004. Geochemical and isotopic (Nd–O) evidence bearing on the origin of late- to postorogenic high-K granitoid rocks in the Western Superior Province: implications for late Archean tectonomagmatic processes. Precambrian Research 132, 303–326.
Wiedenbeck, M., Alle, P., Corfu, F., Griffin, W.L., Meier, M., Oberli, F., Quadt, A.V., Roddick, J.C., Spiegel, W., 1995. Three natural zircon standards for U–Th–Pb, Lu–Hf, trace element and REE analyses. Geostandards and Geoanalytical Research 19, 1–23.
Williams, I.S., 1998. U–Th–Pb geochronology by ion microprobe. In: Mckinbben, M.A., Shanks III, W.C., Ridey, W.I. (Eds.), Applications of Microanalytical Techniques to Understanding Mineralizing Processes: Reviews on Economic. Geology, 7, pp. 1–35.
Windley, B.F., Alexeiev, D., Xiao, W.J., Kroner, A., Badarch, G., 2007. Tectonic models for accretion of the Central Asian Orogenic belt. Journal of the Geological Society of London 164, 31–47.
Woodhead, J.D., Hergt, J.M., Davidson, J.P., Eggins, S.M., 2001. Hafnium isotope evidence for 'conservative' element mobility during subduction zone processes. Earth and Planetary Science Letters 192, 331–346.
Woodhead, J.D., Hergt, J., Shelley, M., Eggins, S., Kemp, R., 2004. Zircon Hf-isotope analysis with an excimer laser, depth profiling, ablation of complex geometries, and concomitant age estimation. Chemical Geology 209, 121–135.
Wu, F.Y., Lin, J.Q., Wilde, S.A., Zhang, X.O., Yang, J.H., 2005. Nature and significance of the Early Cretaceous giant igneous event in eastern China. Earth and Planetary Science Letters 233, 103–119.
Wu, F.Y., Yang, Y.H., Xie, L.W., Yang, J.H., Xu, P., 2006a. Hf isotopic compositions of the standard zircons and baddeleyites used in U–Pb geochronology. Chemical Geology 234, 105–126.
Wu, F.Y., Walker, R.J., Yang, Y.H., Yuan, H.L., Yang, J.H., 2006b. The chemical–temporal evolution of lithospheric mantle underlying the North China Craton. Geochimica et Cosmochimica Acta 70, 5013–5034.
Wu, F.Y., Sun, D.Y., Ge, W.C., Zhang, Y.B., Grant, M.L., Wilde, S.A., Jahn, B.M., 2011. Geochronology of the Phanerozoic granitoids in northeastern China. Journal of Asian Earth Sciences 41, 1–30.
Xiao, L., Clemens, J.D., 2006. Origin of potassic (C-type) adakite magmas: experimental and field constraints. Lithos 95, 399–414.
Xiao, W., Windley, B.F., Hao, J., Zhai, M., 2003. Accretion leading to collision and the Permian Solonker suture, Inner Mongolia, China: termination of the Central Asian orogenic belt. Tectonics 22, 1069 http://dx.doi.org/10.1029/2002TC001484.
Yang, J.H., Wu, F.Y., Shao, J.A., Wilde, S.A., Xie, L.W., Liu, X.M., 2006. Constraints on the timing of uplift of the Yanshan fold and thrust belt, North China Craton. Earth and Planetary Science Letters 246, 336–352.
Yang, J.H., Wu, F.Y., Wilde, S.A., Belousova, E., Griffin, W.L., 2008a. Mesozoic decratonization of the North China block. Geology 36, 467–470.
Yang, J.H., Wu, F.Y., Wilde, S.A., Chen, F.K., Liu, X.M., Xie, L.W., 2008b. Petrogenesis of an alkali syenites-granite-rhyolite suite in the Yanshan fold and thrust belt, eastern North China craton: geochronological, geochemical and Nd–Sr–Hf isotopic evidence for lithospheric thinning. Journal of Petrology 49, 315–351.
Yang, Y.H., Wu, F.Y., Wilde, S.A., Liu, X.M., Zhang, Y.B., Xie, L.W., Yang, J.H., 2009. In situ perovskite Sr–Nd isotopic constraints on the petrogenesis of the Ordovician Mengyin kimberlites in the North China Craton. Chemical Geology 264, 24–42.
Yang, Y.H., Zhang, H.F., Chu, Z.Y., Xie, L.W., Wu, F.Y., 2010. Combined chemical separation of Lu, Hf, Rb, Sr, Sm and Nd from a single rock digest and precise and accurate isotope determinations of Lu–Hf, Rb–Sr and Sm–Nd isotope systems using Multi-Collector ICP-MS and TIMS. International Journal of Mass Spectrometer 290, 120–126.
Ye, H.M., Li, X.H., Li, Z.X., Zhang, C.L., 2008. Age and origin of high Ba–Sr appinite granites at the northwestern margin of the Tibet plateau: implications for early Paleozoic tectonic evolution of the Western Kunlun orogenic belt. Gondwana Research 13, 126–138.
Zhang, X.H., Zhai, M.G., 2010. Magmatism and its metallogenetic effects during the Paleozoic continental crustal construction in northern North China: an overview. Acta Petrologica Sinica 26, 1329–1341.
Zhang, C.H., Song, H.L., Wang, G.H., Yan, D.P., Sun, W.H., 2001. Mesozoic dextral strike-slip structural system in middle segment of intraplate Yanshan orogenic belt, northern China. Journal of China University of Geosciences 26, 464–472.
Zhang, X.H., Li, T.S., Pu, Z.P., 2002. $^{40}Ar/^{39}Ar$ thermochronology of two ductile shear zones from YiwuLüshan, West Liaoning: age constraints on the Mesozoic tectonic events. Chinese Science Bulletin 47, 1113–1118.
Zhang, X.H., Wang, H., Li, T.S., 2005. $^{40}Ar/^{39}Ar$ geochronology of the Faku tectonites: implications for the tectonothermal evolution of the Faku block, northern Liaoning. Science in China, Series D: Earth Sciences 48, 601–612.
Zhang, X.H., Zhang, H.F., Tang, Y.J., Wilde, S.A., Hu, Z.C., 2008a. Geochemistry of Permian bimodal volcanic rocks from Central Inner Mongolia, North China: implication for tectonic setting and Phanerozoic continental growth in Central Asian orogenic belt. Chemical Geology 249, 261–281.
Zhang, X.H., Mao, Q., Zhang, H.F., Wilde, S.A., 2008b. A Jurassic peraluminous leucogranite from Yiwulüshan, western Liaoning, North China Craton: age, origin and tectonic significance. Geological Magazine 145, 305–320.
Zhang, S.H., Zhao, Y., Song, B., Hu, J.M., Liu, S.W., Yang, Y.H., Chen, F.K., Liu, X.M., Liu, J., 2009a. Contrasting late Carboniferous and late Permian–middle Triassic intrusive suites from the northern margin of the North China Craton: geochronology, petro-genesis and tectonic implications. Geological Society of America Bulletin 121, 181–200.
Zhang, S.H., Zhao, Y., Liu, X.C., Liu, D.Y., Chen, F.K., Xie, L.W., Chen, H.H., 2009b. Late Paleozoic to early Mesozoic mafic–ultramafic complexes from the northern North China Block: constraints on the composition and evolution of the lithospheric mantle. Lithos 110, 229–246.
Zhang, X.H., Zhang, H.F., Zhai, M.G., Wilde, S.A., Xie, L.W., 2009. Geochemistry of middle Triassic gabbros from northern Liaoning, North China: origin and tectonic implications. Geological Magazine 146, 540–551.
Zhang, X.H., Zhang, H.F., Jiang, N., Zhai, M.G., Zhang, Y.B., 2010a. Early Devonian alkaline intrusive complex from the northern North China Craton: a petrologic monitor of post-collisional tectonics. Journal of the Geological Society of London 167, 717–730.
Zhang, X.H., Zhang, H.F., Wilde, S.A., Yang, Y.H., Chen, H.H., 2010b. Late Permian to early Triassic mafic to felsic intrusive rocks from North Liaoning, North China: petrogenesis and implication for Phanerozoic continental growth. Lithos 117, 283–306.
Zhang, X.H., Mao, Q., Zhang, H.F., Zhai, M.G., Yang, Y., Hu, Z., 2011a. Mafic and felsic magma interaction during the construction of high-K calc-alkaline plutons within a metacratonic passive margin: the early Permian Guyang batholith from the northern North China Craton. Lithos 125, 569–591.
Zhang, X.H., Wilde, S.A., Zhang, H.F., Zhai, M.G., 2011b. Early Permian high-K calc-alkaline volcanic rocks from northwest Inner Mongolia, North China: geochemistry, origin and tectonic implications. Journal of the Geological Society of London 168, 525–543.
Zhang, X.H., Gao, Y.L., Wang, Z.J., Liu, H., Ma, Y.G., 2012a. Carboniferous appinitic intrusions from the northern North China craton: geochemistry, petrogenesis and tectonic implications. Journal of the Geological Society of London 169 http://dx.doi.org/10.1144/0016-76492011-062.
Zhang, X.H., Yuan, L.L., Xue, F.H., Zhang, Y., 2012b. Contrasting Triassic ferroan granitoids from northwestern Liaoning, North China: magmatic monitor of Mesozoic decratonization and craton-orogen. Lithos 144–145, 12–23.
Zhang, H.F., Zhu, R.X., Santosh, M., Ying, J.F., Su, B.X., Hu, Y., 2012a. Episodic widespread magma underplating beneath the North China Craton in the Phanerozoic: implications for craton destruction. Gondwana Research http://dx.doi.org/10.1016/j.gr.2011.12.006.
Zhang, H.F., Ying, J.F., Santosh, M., Zhao, G.C., 2012b. Episodic growth of Precambrian lower crust beneath the North China Craton: a synthesis. Precambrian Research http://dx.doi.org/10.1016/j.precamres.2011.04.006.
Zhao, G.C., Wilde, S.A., Cawood, P.A., Sun, M., 2001. Archean blocks and their boundaries in the North China Craton: lithological, geochemical, structural and P–T path constraints and tectonic evolution. Precambrian Research 107, 45–73.
Zhao, G.C., Sun, M., Wilde, S.A., Li, S.Z., 2005. Late Archean to Paleoproterozoic evolution of the North China Craton: key issues revisited. Precambrian Research 136, 177–202.
Zhou, X.H., Sun, M., Zhang, G.H., Chen, S.H., 2002. Continental crust and lithospheric mantle interaction beneath North China: isotopic evidence from granulite xenoliths in Hannuoba, Sino-Korean craton. Lithos 62, 111–124.